

Abrupt shifts of productivity and sea ice regimes at the western Barents Sea slope from the Last Glacial Maximum to the Bølling-Allerød interstadial

Denizcan Köseoğlu^{a,*}, Simon T. Belt^a, Jochen Knies^{b,c}

^a Biogeochemistry Research Centre, School of Geography, Earth and Environmental Sciences, Plymouth University, Plymouth, PL4 8AA, UK

^b CAGE – Centre for Arctic Gas Hydrate, Environment and Climate, Department of Geosciences, UiT The Arctic University of Norway, 9037 Tromsø, Norway.

^c Geological Survey of Norway, N-7491 Trondheim, Norway.

*Author for correspondence

E-mail: deniz.koseoglu@plymouth.ac.uk

Alternative e-mail: denizcan.koseoglu@gmail.com

Keywords: Arctic Ocean; Quaternary; Sea ice; Marine biomarkers; HBI; IP₂₅; PIP₂₅; Barents Sea; Coastal polynya; Classification Tree

1 **Abstract**

2 Advanced knowledge of spatio-temporal constraints on the Barents Sea Ice Sheet during
3 the late Weichselian glaciation overshadows relatively limited understanding of seasonal sea
4 ice (experiencing an annual advance-retreat cycle) and primary productivity trends
5 accompanying massive, abrupt climate changes during glacial-deglacial cycles. Such paleo-
6 reconstructions are crucial prerequisites for improved comprehension and prediction of
7 current and future climate change. Here, we investigate sea ice and phytoplankton biomarker
8 distributions in a Barents Sea sediment core covering ca. 25.8–15.4 cal kyr BP to elucidate
9 abrupt shifts of spring–summer sea ice concentrations and relative sympagic–pelagic
10 productivity trends at the southwestern continental slope. Despite significant presence of
11 seasonal sea ice, the Last Glacial Maximum (LGM) and initial shelf edge deglaciation
12 (SEDG) at the core site are characterised by occurrence of productive coastal polynya
13 adjacent to the maximum ice sheet extent. The onset of perennial (i.e. multi-year) ice cover
14 and near-zero productivity during Heinrich Stadial 1 (HS1; ca. 18.0–16.3 cal kyr BP)
15 accompanies significant meltwater fluxes from ice sheet debuitressing and the consequent
16 stagnation of thermohaline circulation. Rapid sea ice retreat and unprecedented pelagic
17 productivity observed after 16.3 cal kyr BP coincides with areal ice sheet deglaciation and is
18 potentially linked to the release of sub-surface heat and nutrient reservoirs, together with
19 reinvigorated deep water circulation following millennial heating of the deep ocean during
20 HS1. We find that a multivariate fingerprinting approach involving assessment of both
21 downcore and surface biomarker distributions is able to distinguish relative ice-algal and
22 pelagic diatom productivity driven by sea ice dynamics.

23 **1. Introduction**

24 Arctic sea ice cover is an integral component of the climate system and exhibits complex
25 interactions with the ocean and the atmosphere. High albedo allows sea ice to effectively
26 reflect incoming solar radiation during the spring and summer months, while extensive areal
27 coverage during winter prevents excessive oceanic heat loss, thus regulating the heat budget
28 across the ocean-atmosphere interface (e.g. Smedsrud et al., 2013). Oceanic convection from
29 brine expulsion during ice formation contributes to the thermohaline overturning circulation
30 (Berger and Jansen, 1995), while occurrence of leads, polynya and seasonal ice melting
31 stratifies the water column, facilitating between 10–55 % of all primary productivity in the
32 Arctic Ocean (Gosselin et al., 1997; Wassmann et al., 1999, 2006). The decline of seasonal
33 sea ice extent (Fetterer et al., 2017), thickness (Lindsay and Schweiger, 2015), and perennial
34 (multi-year) ice fraction (Smedsrud et al., 2017) evident since ca. 1850 AD (Walsh et al.,
35 2017) has accelerated further over the last ca. 40 years. Such a precipitous decline is
36 augmented via positive feedback (Smedsrud et al., 2013) and is likely caused by a
37 combination of anthropogenic warming (Notz and Marotzke, 2012), as well as increasing
38 inflow and temperature of Atlantic Water (AW) (Årthun et al., 2012). The latter is most
39 evident in the seasonally ice-covered Barents Sea, where the North Atlantic Current (NAC)
40 provides ample nutrients for spring-summer primary productivity blooms (e.g. Wassmann et
41 al., 1999, 2006). Higher volume and temperature of AW and multi-decadal recession of the
42 Barents Sea ice cover (Onarheim et al., 2018) are already contributing to earlier ice melt,
43 increased lead/polynya incidence (Willmes and Heinemann, 2016), hastening of spring
44 phytoplankton blooms (Stroeve et al., 2014), and northward intrusion of lower-energy,
45 smaller pelagic species at the expense of ice-obligate algae (Hegseth and Sundfjord, 2008;
46 Assmy et al., 2017; Hoppe et al., 2018) that likely affects survivability and biodiversity of
47 pelagic and benthic communities in the region (Søreide et al., 2013). The motivation of

48 understanding such implications and forecasting development of high-latitude oceans in a
49 warming climate implies paleo-reconstruction of sea ice conditions and associated responses
50 of sympagic and pelagic biota over longer timescales.

51 Such paleo reconstructions can potentially be obtained through the analysis of proxy
52 measures of sympagic and pelagic primary production in sedimentary records whose
53 temporal coverage includes significant shifts in oceanographic and sea ice conditions. Sea ice
54 reconstructions traditionally involve analysis of census data and isotopic composition of
55 calcareous and siliceous microfossils, including foraminifer tests, dinocysts and diatom
56 frustules (de Vernal et al., 2013, and references therein). However, microfossils are
57 susceptible to carbonate and silicate dissolution in corrosive waters formed, for example, via
58 brine rejection during ice formation (Zamelczyk et al., 2014). Such challenges may
59 potentially be circumvented via analysis of certain geochemical lipid biomarkers, such as
60 highly-branched isoprenoids (HBIs; Belt and Müller, 2013; Belt, 2018) and sterols (Volkman,
61 1986), which are often more stable over geologically-significant timescales (e.g. Stein and
62 Fahl, 2013) and can be source-specific (Belt and Müller, 2013; Belt, 2018). A suite of such
63 biomarker proxies representing contrasting primary production sources (e.g. sympagic versus
64 pelagic) may therefore be used to reconstruct environmental variability over temporal
65 windows spanning significant climate shifts. For example, the LGM in the Barents Sea
66 between ca. 26.5–19.0 cal kyr BP (Clark et al., 2009; Peltier and Fairbanks, 2006) and
67 eventual collapse of the Barents Sea Ice Sheet (BSIS) between ca. 18.0–17.5 cal kyr BP
68 (Bauch et al., 2001; Dokken and Jansen, 1999; Elverhøi et al., 1995; Knies et al., 2018) are
69 relevant time intervals for investigating the interactions between AW inflow, Atlantic
70 Meridional Overturning Circulation (AMOC), sea ice concentration, and primary
71 productivity. Geochemical evidence suggests that the LGM and post-deglaciation intervals
72 exhibited heavy seasonal sea ice and near ice-free conditions, respectively, and were

73 punctuated by the Heinrich Stadial 1 (HS1), when harsh glaciomarine conditions and
74 weakened AW inflow prevented growth of biota (e.g. Jennings et al., 2018; Knies et al.,
75 2018; Müller et al., 2009; Müller and Stein, 2014). Such contrasting conditions that
76 characterised these time intervals, coupled with the direct interaction of AW inflow with both
77 the maximum-extent BSIS and the adjacent sea ice margin, make the Late Weichselian
78 Barents Sea key for elucidating the interactions between oceanographic conditions, the sea
79 ice regime, and the associated interplay of sympagic and pelagic primary productivity. Such
80 an investigation could also aid the understanding of potential consequences associated with
81 the projected debuttressing of the contemporary West Antarctic Ice Sheet (WAIS) (Hulbe,
82 2017), for which the Late Weichselian BSIS was previously suggested as a close paleo-
83 analogue (Andreassen and Winsborrow, 2009; Bjarnadottir et al., 2014).

84 The focus of this study was, therefore, to reconstruct sea ice conditions and associated
85 changes in primary productivity at the western Barents Sea continental slope throughout
86 extreme climate shifts spanning ca. 25.8–15.4 cal kyr BP. To achieve this, we quantified a
87 multivariate set of 10 geochemical biomarkers (**Table 1**) representing ice-algal and marine
88 phytoplankton input (**Fig. 1**) in a marine sediment core (**Fig. 2b**) to assess the roles of ice
89 cover and coastal polynya proximal to the BSIS in sustaining both sympagic and pelagic
90 primary productivity from the LGM to the retreat of sea ice cover preceding the Bølling-
91 Allerød (BA) interstadial. Downcore biomarker distributions were compared to those of
92 proximal surface sediments to identify paleo-analogues of contemporary sea ice and
93 productivity settings or, alternatively, determine whether certain intervals within the
94 downcore record represent unique conditions not reproduced in the current climate.

95

96 **2. Biomarker background**

97 HBI isomers are unsaturated hydrocarbons produced exclusively by a relatively narrow range of
98 marine and lacustrine diatoms (Belt and Müller, 2013; Belt, 2018). A C₂₅ HBI discovered in
99 Canadian Arctic sea ice and labelled IP₂₅ (Belt et al., 2007) was confirmed as a seasonal sea
100 ice proxy due to its accumulation during the spring diatom bloom in March–April (Brown et
101 al., 2011) and Arctic sea ice diatom sources (*Pleurosigma* and *Haslea* spp.; Brown et al.,
102 2014b), all of which also contribute to Barents Sea spring blooms (von Quillfeldt, 2000).
103 Notably, at least certain productive sea-ice diatom species abundant in multi-year ice
104 (Syvertsen, 1991; Boetius et al., 2013), such as *Melosira arctica*, do not produce IP₂₅ or any
105 other HBIs. Accordingly, numerous analyses of surface sediments ($n > 850$) spanning the
106 Arctic Ocean showed near-ubiquitous presence of IP₂₅ in seasonally ice-covered locations,
107 and either very low abundance or absence in regions of year-round open water or multi-year
108 ice cover, such as that found in the central Arctic (Xiao et al., 2013). IP₂₅ has since been
109 extensively used for reconstructing past sea ice variability throughout the Arctic Ocean and
110 the Nordic Seas (Belt, 2018, and references therein). An HBI diene (HBI II; Table 1) is co-
111 produced (Brown et al., 2014b) and usually highly correlated (e.g. Cabedo-Sanz et al., 2013;
112 Xiao et al., 2013) with IP₂₅. The latter is often combined with a marine phytoplankton
113 biomarker (e.g. brassicasterol, dinosterol; Volkman, 1986) into the Phytoplankton–IP₂₅ index
114 (PIP₂₅; **Eq. 1** and **Fig. 1**) to obtain semi-quantitative descriptions of sea ice conditions (e.g.
115 Müller et al., 2011; Stein et al., 2017; Xiao et al., 2015). More recently, the calculation of a
116 P_{III}IP₂₅ index using a tri-unsaturated HBI (HBI III; **Table 1** and **Fig. 1**) as the phytoplankton
117 biomarker resulted in semi-quantitative spring sea ice concentration (SpSIC) estimates in the
118 Barents Sea (Belt et al., 2015; Berben et al., 2017; Smik et al., 2016). Further, HBI III and its
119 diastereoisomer (HBI IV; **Table 1** and **Fig. 1**) were recently detected in the pelagic diatom
120 *Rhizosolenia setigera* near Western Svalbard (Belt et al., 2017). Indeed, *R. setigera* is likely
121 the most cosmopolitan among identified producers of trienes III and IV (Belt et al., 2000;

122 Brown et al., 2014a), given its identification as one of most globally abundant diatoms
123 (Leblanc et al., 2012) and the capacity of certain *Rhizosolenia* spp. for active buoyancy
124 control (Joseph et al., 1997) and formation of macroscopic mats under nutrient-replete
125 conditions (Yoder, 1994). Together with high correlation and clear enhancement of both
126 biomarkers near the receding spring sea ice edge (Belt et al., 2015), this supports the use of
127 HBIs III and IV as indicators of pelagic diatom productivity in the Barents Sea. Thus, the
128 availability of a multivariate HBI biomarker set in Barents Sea surface sediments (IP₂₅, HBIs
129 II, III and IV; **Table 1** and **Fig. 1**) recently prompted the development of a classification tree
130 (CT) model of HBI distributions (**Fig. 1**) in surface sediments as a viable method of
131 categorising sea ice conditions over centennial to millennial timescales (Köseoğlu et al.,
132 2018a, 2018b). These investigations showed clear enhancement of pelagic HBIs III and IV
133 relative to sympagic IP₂₅ and HBI II in the productive Barents Sea MIZ, while the reverse
134 was evident under heavy ice cover northeast off Svalbard. The database of HBI
135 concentrations in Barents Sea surface sediments therefore provides an opportunity to
136 determine whether, and to what extent, HBI distributions characteristic of different sea ice
137 regimes in the modern Barents Sea are reproduced within the Late Weichselian sedimentary
138 sequence.

139 To complement the HBI data, we also analysed several sterol lipids, which are ubiquitous
140 components of eukaryotes (Volkman, 1986). In marine settings, the particular diversity of
141 C₂₇–C₂₉ sterols among microorganisms, including microalgae and plankton (Volkman, 2003),
142 has facilitated their use as chemotaxonomic biomarkers of organic matter sources in paleo-
143 environments, including high-latitude shelf seas (e.g. Belt et al., 2013; Knies, 2005). Despite
144 this, few sterols are considered unambiguous biomarkers of specific algal groups as many
145 classes of marine microorganisms contribute the same sterols to the sedimentary budget
146 (Volkman, 1986). For instance, 24-methylcholesta-5,22*E*-dien-3β-ol (epibrassicasterol) and

147 24-methylcholesta-5,24(28)-dien-3 β -ol (24-methylenecholesterol or chalinasterol) are often
148 used as indicators of diatom primary production, despite the fact that the former is often not a
149 major constituent of diatoms (Rampen et al., 2010) and is found in other clades of algae
150 (Volkman, 1986; Volkman et al., 1999). Additionally, epibrassicasterol has been utilised as
151 an indicator of pelagic phytoplankton productivity in ice-covered regions (e.g. Navarro-
152 Rodriguez et al., 2013), in spite of its abundance in sea ice (Belt et al., 2013, 2018) and
153 pennate diatoms (e.g. Rampen et al., 2010). Moreover, diatoms often produce C₂₉ sterols
154 (Belt et al., 2013, 2018; Rampen et al., 2010), such as 24-ethylcholest-5-en-3 β -ol (β -
155 sitosterol) and 24-methylcholest-5-en-3 β -ol (campesterol) traditionally associated with
156 vascular plants (Huang and Meinschein, 1976), which makes distinguishing between marine
157 and terrigenous organic matter in sediments challenging. Even 4-methyl C₃₀ sterols, such as
158 4 α ,23,24-trimethyl-5 α -cholesta-22-en-3 β -ol (dinosterol), traditionally considered to be
159 exclusive to dinoflagellates (Boon et al., 1979) and more specific to marine productivity (e.g.
160 Knies, 2005), have been detected in both sea ice (Nichols et al., 1990) and diatom cultures
161 (*Navicula* spp.; Volkman et al., 1993). Such factors underline the need to consider more
162 source-specific biomarkers, such as HBIs representative of sympagic and pelagic sources, in
163 addition to sterols when decoupling ice-covered and open water conditions in paleo-records
164 (Belt et al., 2015; Smik et al., 2016). Despite their wide distribution across different biota,
165 sterols remain useful indicators of both marine and terrigenous sedimentation, as well as
166 general marine primary productivity, provided such inferences are drawn from a multivariate
167 sterol record further contextualised using other proxy data (Volkman, 1986) or more source-
168 specific biomarkers (such as IP₂₅ and other HBIs). Here, we focus on downcore relative
169 abundance distributions of a multivariate sterol set (**Table 1**), and compare these with surface
170 sediment sterol distributions representative of contrasting sea ice (and productivity)
171 conditions in the modern Barents and Norwegian seas.

172 3. Modern regional setting

173 The warm and saline NAC carries a significant amount of heat into the seasonally ice-
174 covered Barents Sea (Smedsrud et al., 2010), which continues along the western and northern
175 continental margins as the largely sub-surface West Spitsbergen Current (WSC), while the
176 North Cape Current (NCaC) branches out towards Novaya Zemlya and the central Barents
177 Sea (**Fig. 2a**). Fresher coastal water (CW) from the Baltic Sea flows inshore of the NAC with
178 the Norwegian Coastal Current (NCC). Southwest-bound Arctic Water (ArW) enters the
179 Barents Sea with the East Spitsbergen and Persey Currents (ESC and PC, respectively),
180 forming a fresher and colder surface layer around Svalbard (Loeng et al., 1991; Smedsrud et
181 al., 2013). Effective turbulent mixing of warm AW towards the surface during the winter
182 (October–March), when over half of the Barents Sea may be ice-covered (Fetterer et al.,
183 2017), facilitates selective thinning of the ice cover along the path of inflowing AW and
184 keeps a significant portion of western and northern Svalbard shelves ice-free (Ivanov et al.,
185 2012). Ice recession towards the northern shelf break occurs throughout the insolation-
186 triggered melt season during spring and summer (April–September). The interplay of
187 freshwater input and increased light penetration due to melting sea ice stabilises free-floating
188 phytoplankton and AW-carried nutrients within the euphotic zone, developing extensive, but
189 short-lived primary productivity blooms in the MIZ around the retreating ice margin
190 (Wassmann et al., 1999, 2006). The resulting algal biomass fuels energy transfer to higher
191 trophic levels (e.g. zooplankton) and eventually reaches the ocean floor, helping sustain
192 benthic life (Søreide et al., 2013). Further, the development of leads and polynyas coupled
193 with weak stratification from AW-induced melting of sea ice may trigger under-ice pelagic
194 blooms even prior to the melt season (Assmy et al., 2017; Strass and Nöthig, 1996).
195 Sympagic blooms of ice algae develop up to two months prior to seasonal ice retreat as they
196 do not rely on stratification and are triggered by increasing solar insolation in March

197 (Signorini and McClain, 2009). Increasing temperature and volume of inflowing AW has
198 already increased primary productivity by ca. 30% since the 1990’s by reducing sea ice
199 extent and expanding that of the MIZ, prolonging and hastening the bloom season (Arrigo
200 and van Dijken, 2015; Strong and Rigor, 2013). Nonetheless, average phytoplankton biomass
201 at peak bloom is decreasing due to accelerated zooplankton grazing in a warming Barents Sea
202 (Kvile et al., 2016).

203 **4. Materials and methods**

204 *4.1 Sediment material*

205 The 1384 cm long GS14-190-PC01 piston core (71.475° N, 16.165°E; 949 m water
206 depth), hereafter GS14, was recovered aboard the RV “G.O. Sars” on June 3rd, 2014 at the
207 southwestern Barents Sea slope (**Fig. 2b**). A detailed core chronology for the upper 694 cm
208 of the core is available from Knies et al. (2018) and is based on six accelerator mass
209 spectrometry (AMS) ¹⁴C measurements of planktonic and benthic microfossils, including
210 foraminifera and *Thyasira* spp. bivalves. This is supported by an additional six radiocarbon
211 dates transferred to a common depth scale from the gravity core 33-GC08 (hereafter GC08)
212 sampled from the same location as core GS14 using five tie-points inferred from XRF Ca
213 records. The radiocarbon ages were calibrated to calendar ages (cal kyr BP) using the
214 Marine13 curve (Reimer et al., 2013), and no local reservoir age correction was applied
215 ($\Delta R=0$). Finally, Bayesian accumulation age-depth modelling (Bacon 2.2) was used to create
216 the age model (Blaauw and Christen, 2011).

217 In this study, core depths of 11.5–523 cm (ca. 25.8–15.4 cal kyr BP) were investigated,
218 with the age model supported by four and five ¹⁴C AMS dates from cores GS14 and GC08,
219 respectively (**Fig. 3–5**). A total of 131 one centimetre sediment horizons were sampled with
220 10 mL cut-barrel plastic syringes, freeze-dried for 24–48 hours (1 μ bar; -80°C) and frozen in
221 plastic bags at -20°C to preserve sample integrity prior to lipid extraction. While HBIs were

222 extracted and analysed for all 131 horizons, sterol analysis was carried out separately using
223 the same depth interval, but a lower sampling frequency (87 horizons) due to limited
224 availability of material. Sedimentation rates ranged from 12.4 cm kyr⁻¹ to 148.9 cm kyr⁻¹
225 (Knies et al., 2018), resulting in a mean temporal resolution between analysed horizons of 81
226 ± 62 yr for HBIs and 115 ± 74 yr for sterols.

227 To supplement the GS14 downcore analysis, Barents and Norwegian Sea surface
228 sediments ($n = 144$; **Fig. 2b**) representing contrasting contemporary sea ice conditions, and
229 for a larger set of which ($n = 198$) HBI data was recently reported (Köseoğlu et al., 2018a),
230 were re-extracted to obtain sterol distributions. Barents and Norwegian Seas were delineated
231 using the International Council for the Exploration of the Sea (ICES) Ecoregions shapefiles
232 (<http://gis.ices.dk/geonetwork/srv/metadata/4745e824-a612-4a1f-bc56-b540772166eb>).
233 Surface and downcore absolute biomarker concentrations (ng g⁻¹ dry sed.), downcore
234 calibrated horizon ages (cal yr BP), and associated depths (cm) are available from Mendeley
235 Data (doi: <https://doi.org/10.17632/jx97c9nv3k.1>).

236 *4.2 Lipid extraction and analysis*

237 HBIs were extracted according to the methods of Belt et al. (2012), with certain
238 modifications. Briefly, an internal standard (9-octylheptadec-8-ene; 0.1 µg) was added to
239 freeze-dried and homogenized sediment (ca. 2 g), and the total organic extract (TOE) was
240 obtained following repeated sonication and centrifugation with a DCM : MeOH solvent
241 mixture (2:1 v/v; 3 × 2 mL). The solvent was evaporated to dryness at 25°C under N₂, and the
242 TOE was re-suspended in hexane (ca. 1 mL). Elemental sulphur was removed by repeatedly
243 shaking the sample with ca. 1 mL of tetrabutylammonium sulphite reagent (3.39 g in 100 mL
244 of milliQ water saturated with 25 g of anhydrous sodium sulphite) and 2 mL of isopropanol,
245 followed by decanting the supernatant hexane layer into a separate vial (4 × 1 mL). The
246 partially purified extracts were evaporated to dryness (N₂; 25°C), re-suspended in hexane (1

247 mL) and transferred onto hexane-conditioned chromatography columns (3×1 mL of hexane;
248 ca. 1 g of 60–200 μm silica). A hydrocarbon fraction containing HBIs was eluted via hexane
249 (ca. 7 mL), which was evaporated to dryness under N_2 , re-suspended in hexane (ca. 300 μL)
250 and further fractionated into saturated and unsaturated hydrocarbons on Ag-ion
251 chromatography columns (Discovery® Ag-Ion; ca. 0.1 g) by successive elution with hexane
252 (ca. 1 mL) and acetone (ca. 2 mL), respectively. The HBI-containing acetone fractions were
253 evaporated to dryness and transferred to gas chromatographic (GC) vials (300 μL) in hexane.

254 Sterols were extracted following internal standard addition to sediments (5α -androstan-
255 3β -ol; 0.1 μg) and saponification with 5% (m/v) methanolic potassium hydroxide (KOH; 9:1
256 v/v MeOH : milliQ water; 70°C for 60 min). Impurities were partially removed by elution via
257 7:3 DCM : hexane (6 mL) on silica chromatography columns (ca. 1 g of hexane-conditioned
258 silica) and sterols were subsequently collected using 4:1 (v/v) hexane : methyl acetate (ca. 7
259 mL). Following N_2 blowdown (25°C), sterol-containing fractions were derivatised with N,O-
260 bis(trimethylsilyl)trifluoroacetamide (BSTFA; 100 μL ; 70°C for 60 min) and transferred to
261 GC vials (300 μL) in DCM.

262 Analysis of HBIs and sterols was carried out via gas chromatography–mass spectrometry
263 (GC–MS) using established methods (Belt et al., 2012, 2013) with an Agilent 7890 gas
264 chromatograph equipped with the HP_{5MS} fused-silica column (30 m; 0.25 μm film thickness;
265 0.25 mm internal diameter) coupled to an Agilent 5975 series mass spectrometric detector.
266 All biomarkers were identified in total ion current (TIC) mode by comparison of peak
267 retention indices ($\text{RI}_{\text{HP5-MS}} = 2081$ for IP₂₅, 2082 for HBI II, 2044 for HBI III and 2091 for
268 HBI IV) (Belt, 2018, and references therein) and mass spectra to authentic standards and, in
269 the case of sterols, to published data (Boon et al., 1979; Combaut, 1986). Quantification was
270 carried out in single ion monitoring (SIM) and TIC modes for HBIs and sterols, respectively.
271 The resulting peak areas were corrected according to internal standard responses,

272 instrumental response factors (RFs), and sediment mass. Re-calibration of RF values allowed
273 us to quantify additional sterols, updating and extending the GS14 dinosterol record of Knies
274 et al. (2018).

275 4.3 Statistical analysis

276 We used divisive changepoint analysis from the R package ECP (James and
277 Matteson, 2013; R Core Team, 2018) on individual biomarker timeseries to identify
278 significant shifts ($p = 0.005$) in biomarker profiles within the investigated temporal window
279 (**Fig. 3** and **4**). $P_{III}IP_{25}$ values for each horizon were derived using a regional concentration
280 balance factor for the Barents Sea (c -factor = 0.63; **Eq. 1**) with non-zero absolute
281 concentrations (ng g⁻¹ dry sed., shown in square brackets in all equations) of IP_{25} and HBI III.
282 Semi-quantitative estimates of spring sea ice concentrations (SpSIC, %; April–June) were
283 subsequently calculated using the Barents Sea SpSIC– $P_{III}IP_{25}$ calibration (**Eq. 2**) of Smik et
284 al. (2016). The occurrence of summer sea ice (SuSIC, %; July–September) was tentatively
285 inferred using a $P_{III}IP_{25}$ -based SpSIC threshold of ca. 70% ($P_{III}IP_{25} > 0.8$; Smik et al., 2016).
286 Semi-quantitative SpSIC estimates were supplemented with categorical classification of each
287 horizon into marginal (near ice-free waters; <10% SpSIC), intermediate (MIZ conditions with
288 ca. 10–50% SpSIC), and extensive (heavy ice cover characteristic of north-eastern Svalbard;
289 >50% SpSIC) sea ice conditions using the multivariate CT model of Köseoğlu et al. (2018a).
290 CT predictions were derived from percentage contributions of each HBI (IP_{25} , HBIs II, III
291 and IV) to the total (**Eq. 3**) and were not carried out for samples where no HBIs were
292 detected.

$$293 \quad P_{III}IP_{25} = \frac{[IP_{25}]}{([IP_{25}] + [III] \times 0.63)} \#(1)$$

$$294 \quad SpSIC (\%) = \frac{(P_{III}IP_{25} - 0.0692)}{0.0107} \#(2)$$

$$HBI (\%) = \frac{[HBI]}{\sum([IP_{25}], [II], [III], [IV])} \times 100 \#(3)$$

In addition to examining downcore profiles (**Fig. 3** and **4**), the absolute concentration (ng g⁻¹ sed.) and compositional distributions (%; **Eq. 3**) of all biomarkers were examined to identify significant distributional shifts and further assess the general variability of each biomarker throughout the record (**Fig. 6**). Relative distributional changes were additionally compared to modern assemblages observed in Barents Sea surface sediments characterised by contrasting overlying SpSIC and annual open water duration (**Fig. 7**; Belt et al., 2015; Köseoğlu et al., 2018a). The SpSIC database represented April–June SIC spanning the 1988–2007 period, previously used to build the CT model (Köseoğlu et al., 2018a).

5. Results

5.1 Biomarker temporal profiles and distributions in core GS14

Following an initial increase from ca. 25.8 cal kyr BP, IP₂₅ and HBI II concentrations reached their respective peak values of 7.5 and 43.7 ng g⁻¹ by ca. 23.7 cal kyr BP (**Fig. 3a**). This coincided with a similar increase of all six sterols during the same period, which culminated between 24.7–23.7 cal kyr BP. Both sympagic HBIs (i.e. IP₂₅ and HBI II) and all sterols remained at relatively high, but variable concentrations until 18.0 cal kyr BP (**Fig. 3, 4, 6b**), while concentrations of HBI trienes III and IV remained low (0.7 ± 0.5 ng g⁻¹ and 0.6 ± 0.5 ng g⁻¹, respectively; **Fig. 6a**). Accordingly, the HBI assemblage was dominated by IP₂₅ and HBI II, with respective percentage contributions of 13 ± 2% and 80 ± 5%, while HBIs III and IV were only minor constituents throughout the 25.8–18.0 cal kyr BP interval (**Fig. 7a**). This was accompanied by average P_{III}IP₂₅ SpSIC estimates of 74 ± 9% and consistently extensive sea ice conditions predicted by the CT model (**Fig. 3c**). However, SpSIC values < 60% with sporadic summer sea ice occurrence ca. 19.2–18.7 cal kyr BP and CT predictions

318 of intermediate (MIZ-like) sea ice conditions accompanied slight, but abrupt decreases in
319 sympagic HBI and sterol concentrations, with the more distinct changes also highlighted by
320 changepoint analysis (**Fig. 3a, 4**). Finally, examination of the sterol distribution revealed the
321 prevalence of β -sitosterol ($23 \pm 6\%$) and epibrassicasterol ($23 \pm 5\%$), with moderate
322 cholesterol ($18 \pm 3\%$) and chalinasterol ($19 \pm 4\%$), as well as relatively minor campesterol
323 ($10 \pm 2\%$) and dinosterol ($7 \pm 2\%$) until 18.0 cal kyr BP (**Fig. 7b**).

324 Precipitous and abrupt decreases of all biomarker concentrations characterised the
325 18.0–16.3 cal kyr BP interval and were detected by changepoint analysis (**Fig. 3 and 4**).
326 Thus, averaged HBI and sterol concentrations ranged from 0.2–2.2 ng g⁻¹ and 57–182 ng g⁻¹,
327 respectively (**Fig. 6**) despite brief increases in IP₂₅ and HBI II to ca. 2.9 ng g⁻¹ and 10.9 ng g⁻¹,
328 respectively (**Fig. 3a**). The interval was also characterised by the highest SpSIC estimates (ca.
329 90%), summer sea ice occurrence, and CT predictions of extensive sea ice conditions (**Fig.**
330 **3c**). Biomarker percentage distributions remained similar to those observed during the 25.8–
331 18.0 cal kyr BP interval, albeit with more variability and, in case of sterols, prevalence of β -
332 sitosterol alongside cholesterol (**Fig. 7**).

333 An abrupt increase of biomarker concentrations, with significant shifts in percentage
334 distributions and sea ice conditions are evident after ca. 16.3 cal kyr BP. P_{III}IP₂₅-derived
335 SpSIC values dropped to a minimum of $4 \pm 11\%$, and the CT model consistently predicted
336 marginal ice cover or open water conditions (**Fig. 3c**). HBIs III and IV increased by ca. 2
337 orders of magnitude to the highest values observed throughout the record (29.1 ± 24.4 ng g⁻¹
338 and 48.2 ± 41.8 ng g⁻¹, respectively), while IP₂₅ and HBI II remained at respective minimum
339 values of 0.6 ± 0.3 ng g⁻¹ and 3.2 ± 1.5 ng g⁻¹ (**Fig. 6a**). Consequently, HBIs III and IV
340 dominated the HBI distribution during this period, with relative abundances of $33 \pm 8\%$ and
341 $53 \pm 14\%$, respectively (**Fig. 7a**). The sterols experienced a similar, but less pronounced
342 resurgence, with most exhibiting concentrations similar to those observed prior to 18.0 cal

343 kyr BP (**Fig. 4** and **6c**). The greatest concentration increase was observed for cholesterol,
344 which reached a mean value of ca. 2957 ± 930 ng g⁻¹ (**Fig. 4d** and **6b**), a factor ca. three
345 higher than the 25.8–18.0 cal kyr BP average (904 ± 302 ng g⁻¹). Cholesterol therefore
346 dominated the sterol assemblage with $36 \pm 1\%$ relative abundance instead of epibrassicasterol
347 and β -sitosterol, which contributed $22 \pm 2\%$ and $12 \pm 1\%$, respectively. Consistently with the
348 remained of the record, chalinasterol abundance ($21 \pm 2\%$) was comparable to that of
349 epibrassicasterol, while campesterol ($6 \pm 1\%$) and dinosterol ($5 \pm 1\%$) remained minor
350 components (**Fig. 7b**).

351 5.2 Surface sediment biomarker distributions

352 HBI distributions in surface sediments (**Fig. 7a**) characterised by extensive sea ice cover
353 (>50% SpSIC; $n = 23$) were characterised by a distinct prevalence of IP₂₅ and HBI II within
354 the assemblage ($23 \pm 4\%$ and $73 \pm 4\%$, respectively), with minor contribution from HBIs III
355 and IV ($2 \pm 2\%$ and $2 \pm 1\%$, respectively). The contribution of sympagic biomarkers was
356 lower and more variable in the central Barents Sea MIZ ($\leq 50\%$ SpSIC; $n = 36$), with
357 respective percentage abundances of $9 \pm 6\%$ and $42 \pm 22\%$ observed for IP₂₅ and HBI II.
358 Accordingly, pelagic HBIs III and IV comprised a higher $31 \pm 19\%$ and $18 \pm 9\%$ of the
359 assemblage, respectively. Ice-free Barents ($n = 119$) and Norwegian Sea ($n = 20$) locations
360 were characterised almost entirely by HBIs III ($56 \pm 14\%$ and $62 \pm 10\%$, respectively) and IV
361 ($42 \pm 3\%$ and $38 \pm 10\%$, respectively), while only 4 locations close to the annual maximum
362 sea ice edge in the Barents Sea exhibited non-zero IP₂₅ and HBI II.

363 Sterol distributions were mainly defined by the variability of β -sitosterol,
364 epibrassicasterol, and cholesterol in all surface sediments. Conversely, chalinasterol,
365 campesterol, and dinosterol remained minor components (**Fig. 7b**). Extensively ice-covered
366 locations showed a prevalence of β -sitosterol ($25 \pm 5\%$), with comparable, but slightly lower
367 abundances of cholesterol ($21 \pm 4\%$) and epibrassicasterol ($22 \pm 5\%$). Conversely, MIZ and

368 ice-free Barents Sea locations ($n = 26$ and $n = 89$, respectively) exhibited decreased β -
369 sitosterol abundance ($14\text{--}17 \pm 3\text{--}5\%$), with epibrassicasterol ($32\text{--}37 \pm 5\text{--}7\%$) and cholesterol
370 ($28\text{--}29 \pm 5\text{--}11\%$) comprising most of the assemblage. Norwegian Sea sediments ($n = 18$)
371 showed consistent prevalence of cholesterol ($32 \pm 3\%$), with similar epibrassicasterol content
372 ($28 \pm 2\%$) and lower β -sitosterol ($22 \pm 2\%$).

373 **6. Discussion**

374 Biomarker data presented herein allow us to reconstruct seasonal sea ice and productivity
375 variability during climatically contrasting conditions encompassing both growth and decay of
376 the BSIS. To facilitate paleo-interpretation and contextualisation, we delineate the GS14
377 record into discrete time slices, and include a rationale for these in section 6.1. Paleo-
378 interpretation for each time slice is then provided in section 6.2–6.4.

379 *6.1 Identification of time slices for core GS14*

380 Our record is delineated into three main time slices: (i) The LGM and initial shelf edge
381 deglaciation (SEDG) following ice sheet destabilisation (ca. 26.0–18.0 cal kyr BP); (ii) HS1
382 following final BSIS collapse (ca. 18.0–16.3 cal kyr BP); (iii) The retreat of sea ice cover (ca.
383 16.3 cal kyr BP) preceding AMOC recovery and the onset of the Bølling-Allerød (BA)
384 interstadial. The time slice definitions are based on a combination of clear changes of
385 biomarker concentrations (**Fig. 3** and **4**) and percentage distributions (**Fig. 6** and **7**), and the
386 agreement between the timing of these changes in core GS14 and paleoceanographic shifts
387 previously identified in the Barents Sea and other Arctic regions. The definitions of the LGM,
388 SEDG, and the HS1 onset are based on the study of Knies et al. (2018), who infer a BSIS
389 advance to its LGM shelf-edge position at ca. 26.0 cal kyr BP from increased sedimentation
390 rates and IRD deposition. This also agrees with previous global definitions of Peltier and
391 Fairbanks (2006) and Clark et al. (2009), who propose LGM onset at 26 cal kyr BP and 26.5

392 cal kyr BP, respectively. An IRD spike marks the SEDG at ca. 19.5 cal kyr BP, while final
393 BSIS collapse between ca. 18.0–17.7 cal kyr BP is associated with a rapid, meltwater-
394 induced planktic $\delta^{18}\text{O}$ depletion signifying the beginning of HS1 (**Fig. 5**) (Knies et al., 2018)
395 and is also observed in various records from the Barents Sea, the Nordic Seas (Elverhøi et al.,
396 1995; Dokken and Jansen, 1999; Bauch et al., 2001; Weinelt et al., 2003; Müller and Stein,
397 2014), and other Arctic seas (e.g. Jennings et al., 2018). In our study, we additionally note the
398 abrupt decreases of all biomarker concentrations by 18.0 cal kyr BP (**Fig. 3** and **4**), and use
399 this date as the beginning of the HS1. Finally, the post-HS1 deglacial period is defined by
400 significant and contemporaneous changes in biomarker concentrations (**Fig. 3b, 3c** and **4**) and
401 relative abundances (**Fig. 6** and **7**) in core GS14 at ca. 16.3 cal kyr BP.

402 *6.2 BSIS-adjacent productive ice margin during the LGM and SEDG (26–18 cal kyr BP)*

403 Based on high dinosterol and IP_{25} concentrations, Knies et al. (2018) previously
404 provided direct evidence of highly-productive coastal polynyas at the GS14 site during the
405 otherwise harsh glacial conditions of the LGM. Such polynyas initiated by AW upwelling
406 and maintained by powerful katabatic winds from the BSIS were previously suggested to
407 significantly influence Late Weichselian sea ice and primary productivity regimes across the
408 western (Müller et al., 2009; Müller and Stein, 2014; Xiao et al., 2015) and northern Barents
409 Sea margins (Chauhan et al., 2016; Knies et al., 1998, 2018; Nørgaard-Pedersen et al., 2003).
410 Our findings of abundant sympagic biomarkers (IP_{25} and II; **Fig. 3a**) with presence of pelagic
411 HBIs III and IV (**Fig. 3b**) and high sterol concentrations (**Fig. 4**) support the existence of
412 extensive, but seasonal sea ice (**Fig. 3c**), high overall productivity, and vertical stabilisation
413 necessary to maintain pelagic spring and summer blooms at the GS14 site (e.g. Falk-Petersen
414 et al., 2000; Signorini and McClain, 2009; Wassmann et al., 1999). This is further
415 corroborated by the similarity of both the overall HBI and sterol assemblages in our record
416 during the LGM and SEDG to that of northern and north-eastern Svalbard (**Fig. 7**) – an ice-

417 covered region characterised by seasonally open waters during the summer (Fetterer et al.,
418 2017; Köseoğlu et al., 2018a, 2018b; Vare et al., 2010), as well as WSC-mediated winter
419 polynya (Ivanov et al., 2012) and a high overall lead fraction (Willmes and Heinemann,
420 2016) facilitating light penetration and development of under-ice pelagic blooms (Assmy et
421 al., 2017; Strass and Nöthig, 1996). Moreover, average LGM and SEDG concentrations of
422 pelagic HBIs III and IV (0.7 ng g^{-1} and 0.6 ng g^{-1} , respectively) and sterols ($0.37\text{--}1.22 \text{ } \mu\text{g g}^{-1}$)
423 in our record (**Fig. 6**) are also similar to those we observe in surface sediments north and
424 north-east off Svalbard ($0.5\text{--}0.6 \text{ ng g}^{-1}$ and $0.63\text{--}2.67 \text{ } \mu\text{g g}^{-1}$ for HBIs and sterols,
425 respectively). Thus, we confirm the incidence of coastal polynya at the GS14 site throughout
426 26–18 cal kyr BP, which is also potentially associated with previously inferred sub-surface
427 AW inflow in the Nordic Seas throughout ca. 27–22.5 cal kyr BP, at least (Chauhan et al.,
428 2016; Dokken and Hald, 1996; Hebbeln et al. 1994; Knies et al., 1999; Nørgaard-Pedersen et
429 al., 2003; Rasmussen et al., 2007; Rørvik et al., 2013; Vogt et al., 2001). Additionally,
430 several investigations report high primary productivity with seasonally open waters evident
431 from coevally high pelagic and sympagic biomarker concentrations along western Svalbard,
432 Yermak Plateau (e.g. Kremer et al., 2018a, 2018b; Müller et al., 2009; Müller and Stein,
433 2014; Rasmussen et al., 2007) and other Arctic regions (Stein et al., 2017), presence of
434 temperate benthic foraminifera west and north off Svalbard (Chauhan et al., 2016), and
435 decreasing planktonic foraminiferal and IRD abundances from the Fram Strait towards the
436 central Arctic Ocean (Nørgaard-Pedersen et al., 2003).

437 The insolation-induced BSIS destabilisation at the GS14 site began at ca. 19.5 cal kyr
438 BP (Knies et al. 2018), as indicated by increased IRD input; surface meltwater influence was
439 likely absent or limited at this time, as no planktic $\delta^{18}\text{O}$ depletions were observed (**Fig. 5**).
440 High IRD input could have diluted biogenic sedimentation, resulting in the slightly decreased
441 sympagic (e.g. IP_{25}) and pelagic (sterols) primary productivity at the core site (**Fig. 3a–b, 4**).

442 Nonetheless, seasonal sea ice conditions that characterised the earlier LGM (26.0–19.7 cal
443 kyr BP) persisted, with frequent summer sea ice occurrence (**Fig. 3c**).

444 6.3 Productivity termination during Heinrich Stadial HS1 (18.0–16.3 cal kyr BP)

445 Precipitous decreases of all biomarker concentrations to minimum values observed
446 throughout the record (**Fig. 3** and **4**) and maximum P_{III}IP₂₅-derived SpSIC with extensive sea
447 ice conditions predicted by the CT model (**Fig. 3c**) support the presence of closed perennial
448 sea ice cover with near-zero primary productivity at the core site between ca. 18–16.3 cal kyr
449 BP (Knies et al., 2018). While a brief increase in sympagic HBIs to late LGM levels at 17.2
450 cal kyr BP potentially indicates sufficient thinning of sea ice cover to initiate photosynthesis
451 during the summer (**Fig. 3a**), the overall onset of harsh conditions agrees with the widespread
452 collapse of NH ice sheets at ca. 17.5 cal kyr BP following continued increases of summer
453 insolation and sea level (Yokoyama et al., 2000; Clark et al., 2009; Shakun et al., 2012),
454 strong ice stream activity (Winsborrow et al., 2010) and AW-induced weathering of the BSIS
455 grounding line (Hormes et al., 2013). Contemporaneous massive meltwater discharges from
456 icebergs are evidenced between ca. 17.7–16.9 cal kyr BP by depleted planktic $\delta^{18}\text{O}$ and
457 dominance of *N. pachyderma* (sin.) across the Norwegian Sea (Hoff et al., 2016; Rasmussen
458 and Thomsen, 2008; Thornalley et al., 2015), southwestern Barents Sea (Rasmussen et al.,
459 2007) and Svalbard (Chauhan et al., 2016; Jessen et al., 2010; Koç et al., 2002). Accordingly,
460 decreased planktic $\delta^{18}\text{O}$ values observed in the GS14 record after ca. 18.0 cal kyr BP (**Fig. 5**)
461 were previously attributed to meltwater-induced cooling and freshening of surface waters due
462 to BSIS collapse (Knies et al., 2018), promoting stratification and sea ice re-expansion in the
463 Barents Sea. Meltwater influence hampered the AMOC (McManus et al., 2004; Ritz et al.,
464 2013), causing a reduction in NAC-bound AW inflow evident from depleted benthic $\delta^{18}\text{O}$
465 values across the Nordic Seas (Bauch et al., 2001; Knies et al., 2001; Rasmussen and
466 Thomsen, 2008). Thus, our findings support the conclusions of Knies et al. (2018) that the

467 combined influence of cold, low-salinity surface waters, a strongly stratified water column,
468 and a hindered AW inflow into the Barents Sea following BSIS disintegration facilitated
469 perennial sea ice formation and limited the volume and upwelling of deep nutrient-rich
470 waters to the photic zone (**Fig. 8b**). We argue that insufficient nutrient replenishment
471 combined with reduced light penetration through thick multi-year ice following the closing of
472 coastal polynya potentially caused a collapse of microalgal stocks – a scenario previously
473 shown by modelling simulations (Schmittner, 2005) that likely resulted in near-zero
474 biomarker concentrations in our dataset from ca. 18.0–16.3 cal kyr BP (**Fig. 3, 4 and 6**).
475 Indeed, similarly to the LGM, the relative distributions of HBIs (**Fig. 7a**) remain consistent
476 with modern assemblages indicative of extensive sea ice conditions North-East off Svalbard
477 (Köseoğlu et al., 2018a), which suggests that primary productivity was still controlled by sea
478 ice. The sterol distribution, however, slightly deviates from that of the north-eastern Svalbard
479 surface sediments (**Fig. 7b**) due to dominance of cholesterol alongside β -sitosterol. The
480 inhospitable conditions of thick ice cover during the HS1 likely reduced algal biodiversity – a
481 trend observed at higher Arctic latitudes today (Falk-Petersen et al., 1998; Henderson et al.,
482 1998). Thus, the change in sterol distribution probably reflects a shift in the algal assemblage,
483 especially given their ubiquity (Belt et al., 2013; Belt, 2018; Volkman, 2003). For instance,
484 spring blooms in the Central Arctic ocean are often dominated by the cold-adapted diatom *M.*
485 *arctica* (Syvertsen, 1991; Boetius et al., 2013), while at least some *Melosirales* produce both
486 β -sitosterol and cholesterol as the two major sterols (Rampen et al., 2010). In any case, the
487 presence of perennial ice overlying the study area is further substantiated by the absence of
488 significant IRD input (**Fig. 5**) and low sedimentation rates of ca. 12 cm kyr⁻¹ throughout the
489 18.0–16.3 cal kyr BP interval in core GS14 (Knies et al., 2018).

490 *6.4 Ice retreat and intense productivity after 16.3 cal kyr BP*

491 Considerable increases in absolute concentrations of pelagic HBIs (**Fig. 3b** and **6a**) and
492 sterols (**Fig. 4** and **6b**), accompanied by shifts in respective percentage distributions (**Fig. 7**)
493 indicated a general climate amelioration with enhanced primary productivity and SpSIC <
494 10% (**Fig. 3c**) after 16.3 cal kyr BP. Low concentrations of sympagic IP₂₅ and HBI II
495 therefore shift the relative distribution to favour HBIs III and IV, which agrees with the
496 modern HBI assemblage representing nearly ice-free settings with prolonged open water
497 duration (**Fig. 7a**). Together with decreased P_{III}IP₂₅-derived SpSIC with CT predictions of
498 marginal sea ice conditions (**Fig. 3c**; Köseoğlu et al., 2018a; Smik et al., 2016) and an abrupt
499 increase of IRD at ca. 16.3 cal kyr BP (Knies et al., 2018), our evidence suggests limited
500 annual sea ice cover (<10% SpSIC) and sympagic productivity (e.g. Belt et al., 2007; Belt
501 and Müller, 2013; Brown et al., 2014b), with favourable conditions for pelagic blooms and
502 the GS14 site being close to the annual maximum ice edge (Belt et al., 2015, 2017). Rapid
503 sea ice and areal BSIS retreat is also apparent throughout the Barents Sea continental shelves
504 between ca. 16.5–15.5 cal kyr BP, inferred from the abundance of opportunistic benthic
505 foraminifera characteristic of productive waters (Chauhan et al., 2016), increased IRD
506 deposition and meltwater release from sea ice and icebergs (e.g. Chauhan et al., 2016; Jessen
507 et al., 2010; Knies and Stein, 1998; Vogt et al., 2001), as well as high biomarker
508 concentrations (e.g. Müller and Stein, 2014) around Svalbard. Since ca. 17.5 cal kyr BP, a
509 gradual increase in insolation (Berger and Loutre, 1991; Laskar et al., 2004) probably
510 contributed to the areal retreat of the BSIS and reinvigoration of the AMOC at ca. 16 cal kyr
511 BP (McManus et al., 2004; Ritz et al., 2013) following a reduction of glacial meltwater flux
512 also evident from modelling studies (e.g. Liu et al., 2009). The deglaciation was potentially
513 also triggered by progressive aridification of the Arctic during HS1 due to limited ocean-
514 atmosphere heat and moisture exchange through perennial ice cover (e.g. Hormes et al.,
515 2013), which reduced the moisture supply for ice sheet build-up. Ice streams retreated from

516 the western Barents Sea margin due to a shifting BSIS mass balance after ca. 17 cal kyr BP
517 (Winsborrow et al., 2010), which contributed to a separation of the BSIS and FIS in the
518 central Barents Sea (Newton and Huuse, 2017). Thus, we suggest that precipitous sea ice
519 retreat from the western Barents Sea continental slope at ca. 16.3 cal kyr BP coincided with
520 the eastbound areal deglaciation of the BSIS (**Fig. 8c**).

521 Conspicuous enhancement of pelagic HBI concentrations (**Fig. 3b** and **6a**) towards
522 values $>140 \text{ ng g}^{-1}$ is unprecedented both within the GS14 record and the contemporary
523 Barents Sea, where maximum sedimentary concentrations of HBIs III and IV detected in the
524 highly-productive MIZ do not exceed ca. 47 and 22 ng g^{-1} , respectively (Belt et al., 2015;
525 Köseoğlu et al., 2018a). Such a remarkable increase in pelagic diatom productivity at the
526 GS14 site after ca. 16.3 cal kyr is in broad agreement with Wollenburg et al. (2004), who also
527 found that paleoproductivity in relatively fresh surface waters surpassed modern averages at
528 the northern Svalbard margin during this period. Additionally, benthic foraminiferal
529 assemblages along the continental margin adapted to warm AW and increased nutrient
530 availability (e.g. Chauhan et al., 2016). Together, these data suggest the existence of
531 significantly more productive post-HS1 conditions compared to those spanning at least the
532 last several decades of sedimentation in the MIZ (Belt et al., 2015; Köseoğlu et al., 2018a),
533 and are unlikely to be solely attributable to sea ice retreat and establishment of a productive
534 seasonal ice margin following HS1.

535 Several factors could have renewed pelagic productivity. The stratified water column in
536 the Arctic throughout HS1 was initially salinity-controlled due to deglacial meltwater input
537 since ca. 20–19 cal kyr BP (e.g. Chauhan et al., 2016; Hoff et al., 2016; Jennings et al., 2018;
538 Jessen et al., 2010; Rasmussen et al., 2007; Rasmussen and Thomsen, 2008), which
539 hampered the AMOC and NADW formation (Gherardi et al., 2009; McManus et al., 2004),
540 slowing deep water ventilation in the North Atlantic and the Nordic Seas (Thiagarajan et al.,

2014; Thornalley et al., 2015). Thus, a combination of reduced convective heat loss from northbound bottom waters due to strong salinity-driven stratification, and geothermal heating (e.g. Adkins et al., 2005) potentially caused a basin-wide increase of subsurface water temperatures according to proxy-based (Cronin et al., 2012; Thiagarajan et al., 2014) and modelling studies (Liu et al., 2009). Indeed, millennial sub-surface warming of 2–3°C since ca. 19 cal kyr BP is supported by foraminiferal transfer function reconstructions (Rørvik et al., 2013), Δ_{47} clumped isotope data, increased Mg/Ca ratios (Cronin et al., 2012; Thiagarajan et al., 2014; Thornalley et al., 2015), and benthic $\delta^{18}\text{O}$ depletions (e.g. Rasmussen and Thomsen, 2004) across the Nordic Seas. Similar warming along the Barents Sea and Svalbard margins is indicated by intrusion of temperate benthic foraminifera adapted to reduced productivity immediately prior to the HS1 (Chauhan et al., 2016; Rasmussen et al., 2007; Wollenburg et al., 2004), which potentially affected the GS14 site and contributed to BSIS debuttressing, triggering glacial conditions at the onset of HS1 (e.g. Hormes et al., 2013; Marcott et al., 2011). Such accumulation of sub-surface heat in a salinity-stratified water column lowers the density of deep waters – a thermobaric effect which positively scales with pressure – and gradually destabilises the column by reducing the depth threshold at which the cold surface waters become denser than the warm, saline waters below. Once the depth threshold is breached, overturning resumes as the cold surface waters accelerate downwards, while the heat and salt accumulated in the deep waters is rapidly released to the surface ocean (e.g. Adkins et al., 2005). Such phenomena have been recorded in the Norwegian Sea, where subsurface temperatures rapidly decreased between ca. 18–15 cal kyr BP following a period of millennial warming (Rørvik et al., 2013; Thornalley et al., 2015). We therefore suggest that intense, instability- or buoyancy-driven upwelling of warm and saline subsurface waters at the GS14 site could have made massive surface reservoirs of heat and nutrients available (**Fig. 8c**) for seasonal ice melting (**Fig. 3c**) and unprecedented pelagic productivity (**Fig. 3b**)

566 after 16.3 cal kyr BP. Increased nutrient availability and efficient surface enrichment
567 activated by this overturning resumption was potentially maintained by the deepening and
568 intensification of the AMOC towards the Bølling-Allerød warming at ca. 15 cal kyr BP
569 (McManus et al., 2004; Ritz et al., 2013; Shakun et al., 2012). Additionally, in contrast to the
570 slow development of stratification and pelagic productivity in the ice-free southwestern
571 Barents Sea today due to strong NAC- and wind-driven vertical mixing (Wassmann et al.,
572 1999), the post-HS1 productive season at the GS14 site could have been prolonged and
573 hastened by earlier stratification due to meltwater input from sea ice and BSIS retreat
574 (Hormes et al., 2013). Influx of ice and iceberg-entrained terrigenous material from coastal
575 erosion could have provided an additional nutrient supply, as previously noted for the
576 postglacial western (Aagaard-Sørensen et al., 2010) and northern Barents Sea (Knies and
577 Stein, 1998). Thus, a combination of marginal seasonal sea ice, surface warming, hastened
578 meltwater-fuelled stratification, and an augmented nutrient input from terrigenous material
579 and intense upwelling potentially stabilised pelagic species longer in the photic zone and
580 reduced nutritional limitation during the peak bloom, explaining the GS14 productivity trends
581 (**Fig. 8c**). Although it is not feasible to decouple the relative influences of individual factors,
582 the core site was probably characterised by a significantly different productivity regime
583 relative to the ephemeral, nutrient-limited blooms that occur in the modern Barents Sea
584 (Signorini and McClain, 2009), where the phytoplankton productivity increase of recent years
585 is mainly driven by a strengthening AW inflow (Årthun et al., 2012) and reducing sea ice
586 extent (Arrigo and van Dijken, 2015; Assmy et al., 2017), and is not influenced by increased
587 meltwater and terrigenous matter fluxes.

588 High sterol concentrations after ca. 16 cal kyr BP resemble the trend of abruptly
589 increasing pelagic HBI concentrations (**Fig. 3b, 4**) and support our assumption of renewed
590 primary productivity at the core site following precipitous ice retreat (**Fig. 3c, 8c**). While

591 most sterols only reach pre-HS1 values at the core site, cholesterol concentrations increase by
592 a factor of 3 relative to LGM values and dominate the percentage distribution at 36% relative
593 abundance instead of β -sitosterol (**Fig. 6b, 7b**). Similarly to HS1, this could simply be
594 attributable to a switch in the algal assemblage to favour cholesterol production (e.g. by
595 centric diatoms; Rampen et al., 2010). Another explanation is the efficient conversion of algal
596 sterols to cholesterol by auxotrophic consumers, including zooplankton, which potentially
597 flourished after the HS1 due to resumed deep circulation (Gherardi et al., 2009; McManus et
598 al., 2004; Ritz et al., 2013) and global atmospheric-oceanic warming (Shakun et al., 2012).
599 Zooplankton at lower trophic levels extensively feed on pelagic and sympagic algae for
600 growth and reproduction, with increased grazing rates characteristic of warm and highly-
601 productive conditions with large phytoplankton stocks (Falk-Petersen et al., 2000;
602 Tamelander et al., 2008). Contemporary zooplankton communities in the Barents Sea MIZ
603 during peak blooms are dominated by crustaceans, including copepods and krill (e.g. Eriksen
604 et al., 2017), which require a continuous source of cholesterol to maintain their phospholipid
605 membranes and produce offspring (Hassett and Crockett, 2009). Accordingly, cholesterol is
606 invariably the major constituent (usually >50%) of sterol distributions in Arctic and Antarctic
607 crustaceans (Hamm et al., 2001; Mühlebach et al., 1999). Herbivorous and omnivorous
608 arthropods largely rely on chemical conversion of phytosterols to cholesterol, which they
609 cannot biosynthesize (Goad, 1981; Martin-Creuzburg and von Elert, 2009) or obtain in
610 sufficient quantity from an algal diet. Therefore, it is possible that the nutrient-replete and
611 diatom-rich conditions inferred from high pelagic HBI (III and IV) concentrations at the
612 GS14 site after HS1 (**Fig. 3b**) revitalised zooplankton production and phytosterol to
613 cholesterol bioconversion, leading to the proportionally larger increases of the latter sterol
614 (**Fig. 4**). Additionally, our suggestion of a warming water column due to intensive post-HS1
615 circulation of sub-surface heat could have accelerated zooplankton metabolism, switching

616 from temperature-limited to nutrient-limited growth with increased nutritional and
617 reproductive cholesterol requirements (Hassett and Crockett, 2009). Overall, increased
618 phytosterol conversion rates and zooplankton stocks following the post-HS1 climate
619 amelioration represent one plausible mechanism for the switch from a phytosterol- to
620 cholesterol-defined sterol assemblage after 16 cal kyr BP. Notably, however, such a
621 cholesterol-dominated sterol distribution is not reproduced in the contemporary Barents Sea,
622 where epibrassicasterol abundances increase alongside those of cholesterol, and are often
623 higher. Consistent cholesterol prevalence is only observed in the warmer Norwegian Sea
624 (**Fig. 7b**) characterised by significant transport of copepods and krill with the NAC (Falk-
625 Petersen et al., 2000), contributing to their role as major pelagic food web components in the
626 Barents Sea (Aarflot et al., 2017; Eriksen et al., 2017). These observations potentially
627 indicate that the highly-productive post-HS1 interval in the GS14 record is unique and not
628 reproduced in the contemporary Barents Sea, supporting similar suggestions based on the
629 unprecedented increase of pelagic HBIs III and IV, which overshadows that of cholesterol
630 (**Fig. 3b, 4d, and 7**).

631

632 **Conclusions**

633 Geochemical biomarkers in a marine sediment core provided new insights into the
634 abruptly shifting seasonal sea ice conditions and primary productivity regimes on the
635 southwestern Barents Sea slope throughout ca. 26–15 cal kyr BP. We draw the following
636 main outcomes:

- 637 1) The LGM interval and initial SEDG were characterised by extensive sea ice covering the
638 site, with seasonal occurrence of highly-productive coastal polynya. Overall marine
639 productivity was variable, but generally high until 18.0 cal kyr BP.

- 640 2) The onset of perennial sea ice cover during HS1 coincides with widespread NH ice sheet
641 collapse and large meltwater influx at ca. 18.0 cal kyr BP as a result of AW-induced basal
642 melting, atmospheric aridification and increased iceberg calving due to sea level rise.
643 Thus, overall productivity plummeted until ca. 16.3 cal kyr BP as a result of a pan-Arctic
644 meltwater-induced pycnocline, abrupt AMOC weakening and reduced light penetration
645 through newly-formed perennial sea ice.
- 646 3) Coincident with a rapid sea ice retreat to values <10% SpSIC between ca. 16.3–16.1 cal
647 kyr BP, primary productivity exceeded the most productive contemporary conditions in
648 the Barents Sea MIZ. This feature is likely uniquely deglacial and attributable to heat and
649 nutrients released to the surface waters due to thermobaric and/or buoyancy-triggered
650 instabilities following sub-surface warming under weak thermohaline circulation of the
651 HS1. Meltwater input and coastal erosion from the BSIS could have provided an
652 additional nutrient supply to the pelagic environment. We tentatively infer a revitalisation
653 of marine fauna due to vast increases of algal biomass and surface warming.
- 654 4) We note some consistency of relative biomarker distributions downcore with those
655 observed in contrasting sea ice and primary productivity regimes of the contemporary
656 Barents Sea. We are able to decouple sympagic and pelagic primary production using
657 source-specific HBI biomarkers characteristic of ice algal and pelagic diatoms, which
658 indicate that LGM productivity was predominantly ice-based, while post-HS1 production
659 conversely relied on free-floating pelagic algae with minor contribution from sympagic
660 sources. In contrast, sterol concentrations remained similar under seasonal sea ice
661 conditions of the LGM and the post-HS1 deglaciation, and likely represent a mixed algal
662 source.

663 **Acknowledgements**

664 We are grateful to Marta Rodrigo-Gámiz and two anonymous reviewers for their
665 comments, which greatly helped improve the focus and presentation of the manuscript. This
666 research was jointly supported by the Research Council of Norway (Centre of Excellence
667 scheme for CAGE; project 223259) and the University of Plymouth.

668 **Data availability**

669 Datasets related to this article can be found at doi: <http://dx.doi.org/10.17632/jx97c9nv3k.1>,
670 hosted at Mendeley Data.

671

672

673

674

675

676

677

678

679

680

681

682

683

684

685 **References**

- 686 1. Aagaard-Sørensen, S., Husum, K., Hald, M., Knies, J. (2010), 'Paleoceanographic
687 development in the SW Barents Sea during the Late Weichselian–Early Holocene
688 transition', *Quaternary Science Reviews* **29**, pp. 3442–3456, doi:
689 <https://doi.org/10.1016/j.quascirev.2010.08.014>.
- 690 2. Aarflot, J.M., Skjoldal, H.R., Dalpadado, P., Skern-Mauritzen, M. (2017),
691 'Contribution of *Calanus* species to the mesozooplankton biomass in the Barents
692 Sea', *ICES Journal of Marine Science* **75**, pp. 2342 – 2354, doi:
693 <https://doi.org/10.1093/icesjms/fsx221>.
- 694 3. Adkins, J.F., Ingersoll, A.P., Pasquero, C. (2005), 'Rapid climate change and
695 conditional instability of the glacial deep ocean from the thermobaric effect and
696 geothermal heating', *Quaternary Science Reviews* **24**, pp. 581–594, doi:
697 <https://doi.org/10.1016/j.quascirev.2004.11.005>.
- 698 4. Andreassen, K., Winsborrow, M. (2009), 'Signature of ice streaming in Bjørnøyrenna,
699 Polar North Atlantic, through the Pleistocene and implications for ice-stream
700 dynamics', *Annals of Glaciology* **50**, pp. 17–27, doi:
701 <https://doi.org/10.3189/172756409789624238>.
- 702 5. Arrigo, K.R., van Dijken, G.L. (2015), 'Continued increases in Arctic Ocean primary
703 production', *Progress in Oceanography* **136**, pp. 60–70, doi:
704 <https://doi.org/10.1016/j.pocean.2015.05.002>.
- 705 6. Årthun, M., Eldevik, T., Smedsrud, L.H., Skagseth, Ø., Ingvaldsen, R.B. (2012),
706 'Quantifying the Influence of Atlantic Heat on Barents Sea Ice Variability and

707 Retreat’, *Journal of Climate* **25**, pp. 4736–4743, doi: [https://doi.org/10.1175/jcli-d-11-](https://doi.org/10.1175/jcli-d-11-00466.1)
708 [00466.1](https://doi.org/10.1175/jcli-d-11-00466.1).

709 7. Assmy, P., Fernández-Méndez, M., Duarte, P., Meyer, A., Randelhoff, A., Mundy,
710 C.J., Olsen, L.M., Kauko, H.M., Bailey, A., Chierici, M., Cohen, L., Doulgeris, A.P.,
711 Ehn, J.K., Fransson, A., Gerland, S., Hop, H., Hudson, S.R., Hughes, N., Itkin, P.,
712 Johnsen, G., King, J.A., Koch, B.P., Koenig, Z., Kwasniewski, S., Laney, S.R.,
713 Nicolaus, M., Pavlov, A.K., Polashenski, C.M., Provost, C., Rösel, A., Sandbu, M.,
714 Spreen, G., Smedsrud, L.H., Sundfjord, A., Taskjelle, T., Tatarek, A., Wiktor, J.,
715 Wagner, P.M., Wold, A., Steen, H., Granskog, M.A. (2017), 'Leads in Arctic pack ice
716 enable early phytoplankton blooms below snow-covered sea ice’, *Scientific Reports* **7**,
717 article 40850, doi: <https://doi.org/10.1038/srep40850>.

718 8. Bauch, H.A., Erlenkeusser, H., Spielhagen, R.F., Struck, U., Matthiessen, J., Thiede, J.,
719 Heinemeier, J. (2001), ‘A multiproxy reconstruction of the evolution of deep and
720 surface waters in the subarctic Nordic seas over the last 30,000 yr’, *Quaternary*
721 *Science Reviews* **20**, pp. 659–678, doi: [https://doi.org/10.1016/S0277-3791\(00\)00098-](https://doi.org/10.1016/S0277-3791(00)00098-6)
722 [6](https://doi.org/10.1016/S0277-3791(00)00098-6).

723 9. Belt, S.T. (2018), 'Source-specific biomarkers as proxies for Arctic and Antarctic sea
724 ice’, *Organic Geochemistry* **125**, pp. 277–298, doi:
725 <https://doi.org/10.1016/j.orggeochem.2018.10.002>.

726 10. Belt, S.T., Allard, W.G., Massé, G., Robert, J.-M., Rowland, S.J. (2000), ‘Highly
727 branched isoprenoids (HBIs): identification of the most common and abundant
728 sedimentary isomers’, *Geochimica et Cosmochimica Acta* **64**, pp. 3839–3851, doi:
729 [https://doi.org/10.1016/S0016-7037\(00\)00464-6](https://doi.org/10.1016/S0016-7037(00)00464-6).

- 730 11. Belt, S.T., Brown, T.A., Ringrose, A.E., Cabedo-Sanz, P., Mundy, C.J., Gosselin, M.,
731 Poulin, M. (2013), 'Quantitative measurement of the sea ice diatom biomarker IP₂₅
732 and sterols in Arctic sea ice and underlying sediments: Further considerations for
733 palaeo sea ice reconstruction', *Organic Geochemistry* **62**, pp. 33–45, doi:
734 <https://doi.org/10.1016/j.orggeochem.2013.07.002>.
- 735 12. Belt, S.T., Brown, T.A., Rodriguez, A.N., Sanz, P.C., Tonkin, A., Ingle, R. (2012), 'A
736 reproducible method for the extraction, identification and quantification of the Arctic
737 sea ice proxy IP₂₅ from marine sediments', *Analytical Methods* **4**, pp. 705–713, doi:
738 <https://doi.org/10.1039/C2AY05728J>.
- 739 13. Belt, S.T., Brown, T.A., Smik, L., Assmy, P., Mundy, C.J. (2018), 'Sterol
740 identification in floating Arctic sea ice algal aggregates and the Antarctic sea ice
741 diatom *Berkeleya adeliensis*', *Organic Geochemistry* **118**, pp. 1–3, doi:
742 <https://doi.org/10.1016/j.orggeochem.2018.01.008>.
- 743 14. Belt, S.T., Brown, T.A., Smik, L., Tatarek, A., Wiktor, J., Stowasser, G., Assmy, P.,
744 Allen, C.S., Husum, K. (2017), 'Identification of C₂₅ highly branched isoprenoid
745 (HBI) alkenes in diatoms of the genus *Rhizosolenia* in polar and sub-polar marine
746 phytoplankton', *Organic Geochemistry* **110**, pp. 65–72, doi:
747 <https://doi.org/10.1016/j.orggeochem.2017.05.007>.
- 748 15. Belt, S.T., Cabedo-Sanz, P., Smik, L., Navarro-Rodriguez, A., Berben, S.M.P., Knies,
749 J., Husum, K. (2015), 'Identification of paleo Arctic winter sea ice limits and the
750 marginal ice zone: Optimised biomarker-based reconstructions of late Quaternary
751 Arctic sea ice', *Earth and Planetary Science Letters* **431**, pp. 127–139, doi:
752 <https://doi.org/10.1016/j.epsl.2015.09.020>.

- 753 16. Belt, S.T., Massé, G., Rowland, S.J., Poulin, M., Michel, C., LeBlanc, B. (2007), 'A
754 novel chemical fossil of palaeo sea ice: IP₂₅', *Organic Geochemistry* **38**, pp. 16–27,
755 doi: <https://doi.org/10.1016/j.orggeochem.2006.09.013>.
- 756 17. Belt, S.T., Müller, J. (2013), 'The Arctic sea ice biomarker IP₂₅: a review of current
757 understanding, recommendations for future research and applications in palaeo sea ice
758 reconstructions', *Quaternary Science Reviews* **79**, pp. 9–25, doi:
759 <https://doi.org/10.1016/j.quascirev.2012.12.001>.
- 760 18. Berben, S.M.P., Husum, K., Navarro-Rodriguez, A., Belt, S.T., Aagaard-Sørensen, S.
761 (2017), 'Semi-quantitative reconstruction of early to late Holocene spring and summer
762 sea ice conditions in the northern Barents Sea', *Journal of Quaternary Science* **32**, pp.
763 587–603, doi: <https://doi.org/10.1002/jqs.2953>.
- 764 19. Berger, A., Loutre, M.F. (1991), 'Insolation values for the climate of the last 10
765 million years', *Quaternary Science Reviews* **10**, pp. 297–317, doi:
766 [https://doi.org/10.1016/0277-3791\(91\)90033-Q](https://doi.org/10.1016/0277-3791(91)90033-Q).
- 767 20. Berger, W.H., Jansen, E. (1995), 'Younger Dryas episode: Ice collapse and superfjord
768 heat pump', in: Troelstra, S.R., van Hinte, J.E., Ganssen, G.M. (eds.), *The Younger*
769 *Dryas*, North-Holland, Amsterdam, Holland, pp. 61–105.
- 770 21. Bjarnadóttir, L.R., Winsborrow, M.C.M., Andreassen, K. (2014), 'Deglaciation of the
771 central Barents Sea', *Quaternary Science Reviews* **92**, pp. 208–226, doi:
772 <https://doi.org/10.1016/j.quascirev.2013.09.012>.
- 773 22. Blaauw, M., Christen, J.A. (2011), 'Flexible Paleoclimate Age-Depth Models Using
774 an Autoregressive Gamma Process', *Bayesian Analysis* **6**, pp. 457–474, doi:
775 <https://doi.org/10.1214/11-BA618>.

- 776 23. Boetius, A., Albrecht, S., Bakker, K., Bienhold, C., Felden, J., Fernández-Méndez,
777 M., Hendricks, S., Katlein, C., Lalande, C., Krumpen, T., Nicolaus, M., Peeken, I.,
778 Rabe, B., Rogacheva, A., Rybakova, E., Somavilla, R., Wenzhöfer, F. (2013), 'Export
779 of Algal Biomass from the Melting Arctic Sea Ice', *Science* **339**, pp. 1430–1432, doi:
780 <https://doi.org/10.1126/science.1231346>.
- 781 24. Boon, J.J., Rijpstra, W.I.C., De Lange, F., De Leeuw, J.W., Yoshioka, M., Shimizu,
782 Y. (1979), 'Black Sea sterol — a molecular fossil for dinoflagellate blooms', *Nature*
783 **277**, pp. 125–127, doi: <https://doi.org/10.1038/277125a0>.
- 784 25. Brown, T.A., Belt, S.T., Cabedo-Sanz, P. (2014a), 'Identification of a novel di-
785 unsaturated C₂₅ highly branched isoprenoid in the marine tube-dwelling diatom
786 *Berkeleya rutilans*', *Environmental Chemistry Letters* **12**, pp. 455–460, doi:
787 <https://doi.org/10.1007/s10311-014-0472-4>.
- 788 26. Brown, T.A., Belt, S.T., Philippe, B., Mundy, C.J., Massé, G., Poulin, M., Gosselin,
789 M. (2011), 'Temporal and vertical variations of lipid biomarkers during a bottom ice
790 diatom bloom in the Canadian Beaufort Sea: further evidence for the use of the IP₂₅
791 biomarker as a proxy for spring Arctic sea ice', *Polar Biology* **34**, pp. 1857–1868, doi:
792 <https://doi.org/10.1007/s00300-010-0942-5>.
- 793 27. Brown, T.A., Belt, S.T., Tatarek, A., Mundy, C.J. (2014b), 'Source identification of
794 the Arctic sea ice proxy IP₂₅', *Nature Communications* **5**, article 4197, doi:
795 <https://doi.org/10.1038/ncomms5197>.
- 796 28. Cabedo-Sanz, P., Belt, S.T., Knies, J., Husum, K. (2013), 'Identification of contrasting
797 seasonal sea ice conditions during the Younger Dryas', *Quaternary Science Reviews*
798 **79**, pp. 74–86, doi: <https://doi.org/10.1016/j.quascirev.2012.10.028>.

- 799 29. Chauhan, T., Rasmussen, T.L., Noormets, R. (2016), 'Palaeoceanography of the
800 Barents Sea continental margin, north of Nordaustlandet, Svalbard, during the last 74
801 ka', *Boreas* **45**, pp. 76–99, doi: <https://doi.org/10.1111/bor.12135>.
- 802 30. Clark, P.U., Dyke, A.S., Shakun, J.D., Carlson, A.E., Clark, J., Wohlfarth, B.,
803 Mitrovica, J.X., Hostetler, S.W., McCabe, A.M. (2009), 'The Last Glacial Maximum',
804 *Science* **325**, pp. 710–714, doi: <https://doi.org/10.1126/science.1172873>.
- 805 31. Combaut, G. (1986), 'GC-MS of Plant Sterol Analysis', in: Linskens, H.F., Jackson,
806 J.F. (eds.), *Gas Chromatography/Mass Spectrometry*. Springer Berlin Heidelberg,
807 Berlin, Heidelberg, Germany, pp. 121–133.
- 808 32. Cronin, T.M., Dwyer, G.S., Farmer, J., Bauch, H.A., Spielhagen, R.F., Jakobsson, M.,
809 Nilsson, J., Briggs Jr, W.M., Stepanova, A. (2012), 'Deep Arctic Ocean warming
810 during the last glacial cycle', *Nature Geoscience* **5**, pp. 631–634, doi:
811 <https://doi.org/10.1038/ngeo1557>.
- 812 33. De Vernal, A., Gersonde, R., Goosse, H., Seidenkrantz, M.-S., Wolff, E.W. (2013),
813 'Sea ice in the paleoclimate system: the challenge of reconstructing sea ice from
814 proxies – an introduction', *Quaternary Science Reviews* **78**, pp. 1–8, doi:
815 <https://doi.org/10.1016/j.quascirev.2013.08.009>.
- 816 34. Dokken, T.M., Hald, M. (1996), 'Rapid climatic shifts during isotope stages 2–4 in
817 the Polar North Atlantic', *Geology* **24**, pp. 599–602, doi:
818 [https://doi.org/10.1130/0091-7613\(1996\)024<0599:RCSDIS>2.3.CO;2](https://doi.org/10.1130/0091-7613(1996)024<0599:RCSDIS>2.3.CO;2).

- 819 35. Dokken, T.M., Jansen, E. (1999), ‘Rapid changes in the mechanism of ocean
820 convection during the last glacial period’, *Nature* **401**, pp. 458–461, doi:
821 <https://doi.org/10.1038/46753>.
- 822 36. Elverhøi, A., Andersen, E.S., Dokken, T., Hebbeln, D., Spielhagen, R., Svendsen, J.I.,
823 Sørflaten, M., Rørnes, A., Hald, M., Forsberg, C.F. (1995), ‘The Growth and Decay
824 of the Late Weichselian Ice Sheet in Western Svalbard and Adjacent Areas Based on
825 Provenance Studies of Marine Sediments’, *Quaternary Research* **44**, pp. 303–316,
826 doi: <https://doi.org/10.1006/qres.1995.1076>.
- 827 37. Eriksen, E., Skjoldal, H.R., Gjøsæter, H., Primicerio, R. (2017), ‘Spatial and temporal
828 changes in the Barents Sea pelagic compartment during the recent warming’,
829 *Progress in Oceanography* **151**, pp. 206–226, doi:
830 <https://doi.org/10.1016/j.pocean.2016.12.009>.
- 831 38. Falk-Petersen, S., Hop, H., Budgell, W.P., Hegseth, E.N., Korsnes, R., Løyning, T.B.,
832 Børre Ørbæk, J., Kawamura, T., Shirasawa, K. (2000), ‘Physical and ecological
833 processes in the marginal ice zone of the northern Barents Sea during the summer
834 melt period’, *Journal of Marine Systems* **27**, pp. 131–159, doi:
835 [https://doi.org/10.1016/S0924-7963\(00\)00064-6](https://doi.org/10.1016/S0924-7963(00)00064-6).
- 836 39. Falk-Petersen, S., Sargent, J.R., Henderson, J., Hegseth, E.N., Hop, H., Okolodkov,
837 Y.B. (1998), ‘Lipids and fatty acids in ice algae and phytoplankton from the Marginal
838 Ice Zone in the Barents Sea’, *Polar Biology* **20**, pp. 41–47, doi:
839 <https://doi.org/10.1007/s003000050274>.
- 840 40. Fetterer, F., Knowles, K., Meier, W., Savoie, M., Windnagel A.K. (2017, updated
841 daily), *Sea Ice Index, Version 3*. NSIDC: National Snow and Ice Data Center,

- 842 Boulder, Colorado, USA, doi: <https://doi.org/10.7265/N5K072F8> (accessed
843 09.04.2019).
- 844 41. Gherardi, J.-M., Labeyrie, L., Nave, S., Francois, R., McManus, J.F., Cortijo, E.
845 (2009), 'Glacial-interglacial circulation changes inferred from $^{231}\text{Pa}/^{230}\text{Th}$ sedimentary
846 record in the North Atlantic region', *Paleoceanography* **24**, article PA2204, doi:
847 <https://doi.org/10.1029/2008PA001696>.
- 848 42. Goad, L.J. (1981), 'Sterol biosynthesis and metabolism in marine invertebrates', *Pure*
849 *& Applied Chemistry* **51**, pp. 837–852, doi:
850 <https://doi.org/10.1351/pac198153040837>.
- 851 43. Gosselin, M., Levasseur, M., Wheeler, P.A., Horner, R.A., Booth, B.C. (1997), 'New
852 measurements of phytoplankton and ice algal production in the Arctic Ocean', *Deep*
853 *Sea Research Part II: Topical Studies in Oceanography* **44**, pp. 1623–1644, doi:
854 [https://doi.org/10.1016/S0967-0645\(97\)00054-4](https://doi.org/10.1016/S0967-0645(97)00054-4).
- 855 44. Hamm, C., Reigstad, M., Riser, C.W., Mühlebach, A., Wassmann, P. (2001), 'On the
856 trophic fate of *Phaeocystis pouchetii*. VII. Sterols and fatty acids reveal sedimentation
857 of *P. pouchetii*-derived organic matter via krill fecal strings', *Marine Ecology*
858 *Progress Series* **209**, pp. 55–69, doi: <https://doi.org/10.3354/meps209055>.
- 859 45. Hassett, R.P., Crockett, E.L. (2009), 'Habitat temperature is an important determinant
860 of cholesterol contents in copepods', *Journal of Experimental Biology* **212**, pp. 71–77,
861 doi: <https://doi.org/10.1242/jeb.020552>.

- 862 46. Hebbeln, D., Dokken, T., Andersen, E.S., Hald, M., Elverhøi, A. (1994), ‘Moisture
863 supply to northern ice-sheet growth during the Last Glacial Maximum’, *Nature* **370**,
864 pp. 357–360, doi: <https://doi.org/10.1038/370357a0>.
- 865 47. Hegseth, E.N., Sundfjord, A. (2008), 'Intrusion and blooming of Atlantic
866 phytoplankton species in the high Arctic', *Journal of Marine Systems* **74**, pp. 108–
867 119, doi: <https://doi.org/10.1016/j.jmarsys.2007.11.011>.
- 868 48. Henderson, R.J., Hegseth, E.N., Park, M.T. (1998), 'Seasonal variation in lipid and
869 fatty acid composition of ice algae from the Barents Sea', *Polar Biology* **20**, pp. 48–
870 55, doi: <https://doi.org/10.1007/s003000050275>.
- 871 49. Hoff, U., Rasmussen, T.L., Stein, R., Ezat, M.M., Fahl, K. (2016), 'Sea ice and
872 millennial-scale climate variability in the Nordic seas 90 kyr ago to present', *Nature*
873 *Communications* **7**, article 12247, doi: <https://doi.org/10.1038/ncomms12247>.
- 874 50. Hoppe, C.J.M., Flintrop, C.M., Rost, B. (2018), 'The Arctic picoeukaryote
875 *Micromonas pusilla* benefits synergistically from warming and ocean acidification',
876 *Biogeosciences* **15**, pp. 4353–4365, doi: <https://doi.org/10.5194/bg-15-4353-2018>.
- 877 51. Hormes, A., Gjermundsen, E.F., Rasmussen, T.L. (2013), 'From mountain top to the
878 deep sea – Deglaciation in 4D of the northwestern Barents Sea ice sheet', *Quaternary*
879 *Science Reviews* **75**, pp. 78–99, doi: <https://doi.org/10.1016/j.quascirev.2013.04.009>.
- 880 52. Huang, W.Y., Meinschein, W.G. (1976), 'Sterols as source indicators of organic
881 materials in sediments', *Geochimica et Cosmochimica Acta* **40**, pp. 323–330, doi:
882 [https://doi.org/10.1016/0016-7037\(76\)90210-6](https://doi.org/10.1016/0016-7037(76)90210-6).

- 883 53. Hughes, A.L.C., Gyllencreutz, R., Lohne, Ø.S., Mangerud, J., Svendsen, J.I. (2016),
884 'The last Eurasian ice sheets – a chronological database and time-slice reconstruction,
885 DATED-1', *Boreas* **45**, pp. 1–45, doi: <https://doi.org/10.1111/bor.12142>.
- 886 54. Hulbe, C. (2017), 'Is ice sheet collapse in West Antarctica unstoppable?', *Science* **356**,
887 pp. 910–911, doi: <https://doi.org/10.1126/science.aam9728>.
- 888 55. Ivanov, V.V., Alexeev, V.A., Repina, I., Koldunov, N.V., Smirnov, A. (2012),
889 'Tracing Atlantic Water Signature in the Arctic Sea Ice Cover East of Svalbard',
890 *Advances in Meteorology* **2012**, article 201818, doi:
891 <http://dx.doi.org/10.1155/2012/201818>.
- 892 56. James, N.A., Matteson, D.S. (2013), 'Ecp: An R Package for Nonparametric Multiple
893 Change Point Analysis of Multivariate Data', *Journal of Statistical Software* **62**, pp.
894 1–25, doi: <https://doi.org/10.18637/jss.v062.i07>.
- 895 57. Jennings, A.E., Andrews, J.T., Ó Cofaigh, C., St-Onge, G., Belt, S., Cabedo-Sanz, P.,
896 Pearce, C., Hillaire-Marcel, C., Calvin Campbell, D. (2018), 'Baffin Bay
897 paleoenvironments in the LGM and HS1: Resolving the ice-shelf question', *Marine*
898 *Geology* **402**, pp. 5–16, doi: <https://doi.org/10.1016/j.margeo.2017.09.002>.
- 899 58. Jessen, S.P., Rasmussen, T.L., Nielsen, T., Solheim, A. (2010), 'A new Late
900 Weichselian and Holocene marine chronology for the western Svalbard slope 30,000–
901 0 cal years BP', *Quaternary Science Reviews* **29**, pp. 1301–1312, doi:
902 <https://doi.org/10.1016/j.quascirev.2010.02.020>.

- 903 59. Joseph, L., Villareal, T.A., Lipschultz, F. (1997), ‘A high sensitivity nitrate reductase
904 assay and its application to vertically migrating *Rhizosolenia* mats’, *Aquatic*
905 *Microbial Ecology* **12**, pp. 95–104, doi: <https://doi.org/10.3354/ame012095>.
- 906 60. Knies, J. (2005), 'Climate-induced changes in sedimentary regimes for organic matter
907 supply on the continental shelf off northern Norway’, *Geochimica et Cosmochimica*
908 *Acta* **69**, pp. 4631–4647, doi: <https://doi.org/10.1016/j.gca.2005.05.014>.
- 909 61. Knies, J., Kleiber, H.-P., Matthiessen, J., Müller, C., Nowaczyk, N. (2001), 'Marine
910 ice-rafted debris records constrain maximum extent of Saalian and Weichselian ice-
911 sheets along the northern Eurasian margin’, *Global and Planetary Change* **31**, pp. 45–
912 64, doi: [https://doi.org/10.1016/S0921-8181\(01\)00112-6](https://doi.org/10.1016/S0921-8181(01)00112-6).
- 913 62. Knies, J., Köseoğlu, D., Rise, L., Baeten, N., Bellec, V.K., Bøe, R., Klug, M., Panieri,
914 G., Jernas, P.E., Belt, S.T. (2018), 'Nordic Seas polynyas and their role in
915 preconditioning marine productivity during the Last Glacial Maximum’, *Nature*
916 *Communications* **9**, article 3959, doi: <https://doi.org/10.1038/s41467-018-06252-8>.
- 917 63. Knies, J., Stein, R. (1998), 'New aspects of organic carbon deposition and its
918 paleoceanographic implications along the northern Barents Sea margin during the last
919 30,000 years’, *Paleoceanography* **13**, pp. 384–394, doi:
920 <https://doi.org/10.1029/98PA01501>.
- 921 64. Knies, J., Vogt, C., Stein, R. (1999), 'Late Quaternary growth and decay of the
922 Svalbard/Barents Sea ice sheet and paleoceanographic evolution in the adjacent Arctic
923 Ocean’, *Geo-Marine Letters* **18**, pp. 195–202, doi:
924 <https://doi.org/10.1007/s003670050068>.

- 925 65. Koç, N., Klitgaard-Kristensen, D., Hasle, K., Forsberg, C.F., Solheim, A. (2002),
926 'Late glacial palaeoceanography of Hinlopen Strait, northern Svalbard', *Polar*
927 *Research* **21**, pp. 307–314, doi: <https://doi.org/10.3402/polar.v21i2.6492>.
- 928 66. Köseoğlu, D., Belt, S.T., Husum, K., Knies, J. (2018b), 'An assessment of biomarker-
929 based multivariate classification methods versus the PIP₂₅ index for paleo Arctic sea
930 ice reconstruction', *Organic Geochemistry* **125**, pp. 82–94, doi:
931 <https://doi.org/10.1016/j.orggeochem.2018.08.014>.
- 932 67. Köseoğlu, D., Belt, S.T., Smik, L., Yao, H., Panieri, G., Knies, J. (2018a),
933 'Complementary biomarker-based methods for characterising Arctic sea ice
934 conditions: A case study comparison between multivariate analysis and the PIP₂₅
935 index', *Geochimica et Cosmochimica Acta* **222**, pp. 406–420, doi:
936 <https://doi.org/10.1016/j.gca.2017.11.001>.
- 937 68. Kremer, A., Stein, R., Fahl, K., Bauch, H., Mackensen, A., Niessen, F. (2018a), 'A
938 190-ka biomarker record revealing interactions between sea ice, Atlantic Water
939 inflow and ice sheet activity in eastern Fram Strait', *Arktos* **4**, article 22, doi:
940 <https://doi.org/10.1007/s41063-018-0052-0>.
- 941 69. Kremer, A., Stein, R., Fahl, K., Ji, Z., Yang, Z., Wiers, S., Matthiessen, J., Forwick,
942 M., Löwemark, L., O'Regan, M., Chen, J., Snowball, I. (2018b), 'Changes in sea ice
943 cover and ice sheet extent at the Yermak Plateau during the last 160 ka –
944 Reconstructions from biomarker records', *Quaternary Science Reviews* **182**, pp. 93–
945 108, doi: <https://doi.org/10.1016/j.quascirev.2017.12.016>.
- 946 70. Kvile, K.Ø., Langangen, Ø., Prokopchuk, I., Stenseth, N.C., Stige, L.C. (2016),
947 'Disentangling the mechanisms behind climate effects on zooplankton', *Proceedings*

- 948 of the *National Academy of Sciences* **113**, pp. 1841–1846, doi:
949 <https://doi.org/10.1073/pnas.1525130113>.
- 950 71. Laskar, J., Robutel, P., Joutel, F., Gastineau, M., Correia, A.C.M., Levrard, B. (2004),
951 'A long-term numerical solution for the insolation quantities of the Earth', *Astronomy*
952 & *Astrophysics* **428**, pp. 261–285, doi: <https://doi.org/10.1051/0004-6361:20041335>.
- 953 72. Leblanc, K., Aristegui, J., Armand, L., Assmy, P., Beker, B., Bode, A., Breton, E.,
954 Cornet, V., Gibson, J., Gosselin, M.-P., Kopczynska, E.E., Marshall, H., Peloquin, J.,
955 Piontkovski, S., Poulton, A.J., Queguiner, B., Schiebel, R., Shipe, R., Stefels, J., van
956 Leeuwe, M.A., Varela, M., Widdicombe, C., Yallop, M. (2012), 'A global diatom
957 database – abundance, biovolume and biomass in the world ocean', *Earth System*
958 *Science Data* **4**, pp. 149–165, doi: <https://doi.org/10.5194/essd-4-149-2012>.
- 959 73. Lindsay, R., Schweiger, A. (2015), 'Arctic sea ice thickness loss determined using
960 subsurface, aircraft, and satellite observations', *The Cryosphere* **9**, pp. 269–283, doi:
961 <https://doi.org/10.5194/tc-9-269-2015>.
- 962 74. Liu, Z., Otto-Bliesner, B.L., He, F., Brady, E.C., Tomas, R., Clark, P.U., Carlson,
963 A.E., Lynch-Stieglitz, J., Curry, W., Brook, E., Erickson, D., Jacob, R., Kutzbach, J.,
964 Cheng, J. (2009), 'Transient Simulation of Last Deglaciation with a New Mechanism
965 for Bølling-Allerød Warming', *Science* **325**, pp. 310–314, doi:
966 <https://doi.org/10.1126/science.1171041>.
- 967 75. Loeng, H. (1991), 'Features of the physical oceanographic conditions of the Barents
968 Sea', *Polar Research* **10**, pp. 5–18, doi: <https://doi.org/10.3402/polar.v10i1.6723>.

- 969 76. Marcott, S.A., Clark, P.U., Padman, L., Klinkhammer, G.P., Springer, S.R., Liu, Z.,
970 Otto-Bliesner, B.L., Carlson, A.E., Ungerer, A., Padman, J., He, F., Cheng, J.,
971 Schmittner, A. (2011), 'Ice-shelf collapse from subsurface warming as a trigger for
972 Heinrich events', *Proceedings of the National Academy of Sciences* **108**, pp. 13415–
973 13419, doi: <https://doi.org/10.1073/pnas.1104772108>.
- 974 77. Martin-Creuzburg, D., von Elert, E. (2009), 'Ecological significance of sterols in
975 aquatic food webs', in: Kainz, M., Brett, M.T., Arts, M.T. (eds.), *Lipids in Aquatic*
976 *Ecosystems*. Springer New York, New York, USA, pp. 43–64, doi:
977 https://doi.org/10.1007/978-0-387-89366-2_3.
- 978 78. McManus, J.F., Francois, R., Gherardi, J.M., Keigwin, L.D., Brown-Leger, S. (2004),
979 'Collapse and rapid resumption of Atlantic meridional circulation linked to deglacial
980 climate changes', *Nature* **428**, pp. 834–837, doi: <https://doi.org/10.1038/nature02494>.
- 981 79. Mühlebach, A., Albers, C., Kattner, G. (1999), 'Differences in the sterol composition
982 of dominant antarctic zooplankton', *Lipids* **34**, pp. 45–51, doi:
983 <https://doi.org/10.1007/s11745-999-336-1>.
- 984 80. Müller, J., Massé, G., Stein, R., Belt, S.T. (2009), 'Variability of sea-ice conditions in
985 the Fram Strait over the past 30,000 years', *Nature Geoscience* **2**, pp. 772–776, doi:
986 <https://doi.org/10.1038/ngeo665>.
- 987 81. Müller, J., Stein, R. (2014), 'High-resolution record of late glacial and deglacial sea
988 ice changes in Fram Strait corroborates ice–ocean interactions during abrupt climate
989 shifts', *Earth and Planetary Science Letters* **403**, pp. 446–455, doi:
990 <https://doi.org/10.1016/j.epsl.2014.07.016>.

- 991 82. Müller, J., Wagner, A., Fahl, K., Stein, R., Prange, M., Lohmann, G. (2011), 'Towards
992 quantitative sea ice reconstructions in the northern North Atlantic: A combined
993 biomarker and numerical modelling approach', *Earth and Planetary Science Letters*
994 **306**, pp. 137–148, doi: <https://doi.org/10.1016/j.epsl.2011.04.011>.
- 995 83. Navarro-Rodriguez, A., Belt, S.T., Knies, J., Brown, T.A. (2013), 'Mapping recent sea
996 ice conditions in the Barents Sea using the proxy biomarker IP₂₅: implications for
997 palaeo sea ice reconstructions', *Quaternary Science Reviews* **79**, pp. 26–39, doi:
998 <https://doi.org/10.1016/j.quascirev.2012.11.025>.
- 999 84. Newton, A.M.W., Huuse, M. (2017), 'Glacial geomorphology of the central Barents
1000 Sea: Implications for the dynamic deglaciation of the Barents Sea Ice Sheet', *Marine*
1001 *Geology* **387**, pp. 114–131, doi: <https://doi.org/10.1016/j.margeo.2017.04.001>.
- 1002 85. Nichols, P.D., Palmisano, A.C., Rayner, M.S., Smith, G.A., White, D.C. (1990),
1003 'Occurrence of novel C₃₀ sterols in Antarctic sea-ice diatom communities during a
1004 spring bloom', *Organic Geochemistry* **15**, pp. 503–508, doi:
1005 [https://doi.org/10.1016/0146-6380\(90\)90096-I](https://doi.org/10.1016/0146-6380(90)90096-I).
- 1006 86. Nørgaard-Pedersen, N., Spielhagen, R.F., Erlenkeuser, H., Grootes, P.M.,
1007 Heinemeier, J., Knies, J. (2003), 'Arctic Ocean during the Last Glacial Maximum:
1008 Atlantic and polar domains of surface water mass distribution and ice cover',
1009 *Paleoceanography* **18**, article 1063, doi: <https://doi.org/10.1029/2002PA000781>.
- 1010 87. Notz, D., Marotzke, J. (2012), 'Observations reveal external driver for Arctic sea-ice
1011 retreat', *Geophysical Research Letters* **39**, article L08502, doi:
1012 <https://doi.org/10.1029/2012GL051094>.

- 1013 88. Onarheim, I.H., Eldevik, T., Smedsrud, L.H., Stroeve, J.C. (2018), 'Seasonal and
1014 Regional Manifestation of Arctic Sea Ice Loss', *Journal of Climate* **31**, pp. 4917–
1015 4932, doi: <https://doi.org/10.1175/jcli-d-17-0427.1>.
- 1016 89. Peltier, W.R., Fairbanks, W.G. (2006), 'Global glacial ice volume and Last Glacial
1017 Maximum duration from an extended Barbados sea level record', *Quaternary Science*
1018 *Reviews* **25**, pp. 3322–3337, doi: <https://doi.org/10.1016/j.quascirev.2006.04.010>.
- 1019 90. R Core Team (2018), *R: A Language and Environment for Statistical Computing*. R
1020 Foundation for Statistical Computing, Vienna.
- 1021 91. Rampen, S.W., Abbas, B.A., Schouten, S., Sinninghe Damste, J.S. (2010), 'A
1022 comprehensive study of sterols in marine diatoms (Bacillariophyta): Implications for
1023 their use as tracers for diatom productivity', *Limnology and Oceanography* **55**, pp.
1024 91–105, doi: <https://doi.org/10.4319/lo.2010.55.1.0091>.
- 1025 92. Rasmussen, T.L., Thomsen, E. (2004), 'The role of the North Atlantic Drift in the
1026 millennial timescale glacial climate fluctuations', *Palaeogeography,*
1027 *Palaeoclimatology, Palaeoecology* **210**, pp. 101–116, doi:
1028 <https://doi.org/10.1016/j.palaeo.2004.04.005>.
- 1029 93. Rasmussen, T.L., Thomsen, E. (2008), 'Warm Atlantic surface water inflow to the
1030 Nordic seas 34–10 calibrated ka B.P.', *Paleoceanography* **23**, article PA1201, doi:
1031 <https://doi.org/10.1029/2007PA001453>.
- 1032 94. Rasmussen, T.L., Thomsen, E., Ślubowska, M.A., Jessen, S., Solheim, A., Koç, N.
1033 (2007), 'Paleoceanographic evolution of the SW Svalbard margin (76°N) since 20,000

- 1034 ^{14}C yr BP’, *Quaternary Research* **67**, pp. 100–114, doi:
1035 <https://doi.org/10.1016/j.yqres.2006.07.002>.
- 1036 95. Reimer, P., Bard, E., Bayliss, A., Beck, J., Blackwell, P., Ramsey, C., Van der Plicht,
1037 J. (2013), ‘IntCal13 and Marine13 Radiocarbon Age Calibration Curves 0–50,000
1038 Years cal BP’, *Radiocarbon* **55**, pp. 1869–1887, doi:
1039 https://doi.org/10.2458/azu_js_rc.55.16947.
- 1040 96. Ringrose, A.E. (2012), *Temporal and vertical distributions of IP₂₅ and other lipid*
1041 *biomarkers in sea ice from Resolute Bay, Nunavut, Canada*, M.Phil. thesis, University
1042 of Plymouth, Plymouth, UK.
- 1043 97. Ritz, S.P., Stocker, T.F., Grimalt, J.O., Meniel, L., Timmermann, A. (2013),
1044 ‘Estimated strength of the Atlantic overturning circulation during the last
1045 deglaciation’, *Nature Geoscience* **6**, pp. 208–212, doi:
1046 <https://doi.org/10.1038/ngeo1723>.
- 1047 98. Rontani, J.-F., Belt, S.T., Brown, T.A., Amiriaux, R., Gosselin, M., Vaultier, F.,
1048 Mundy, C.J. (2016), ‘Monitoring abiotic degradation in sinking versus suspended
1049 Arctic sea ice algae during a spring ice melt using specific lipid oxidation tracers’,
1050 *Organic Geochemistry* **98**, pp. 82–97, doi:
1051 <https://doi.org/10.1016/j.orggeochem.2016.05.016>.
- 1052 99. Rontani, J.-F., Belt, S.T., Brown, T.A., Vaultier, F., Mundy, C.J. (2014a), ‘Sequential
1053 photo- and autoxidation of diatom lipids in Arctic sea ice’, *Organic Geochemistry* **77**,
1054 pp. 59–71, doi: <https://doi.org/10.1016/j.orggeochem.2014.09.009>.

- 1055 100. Rontani, J.-F., Belt, S.T., Vaultier, F., Brown, T.A. (2011), ‘Visible light induced
1056 photo-oxidation of highly branched isoprenoid (HBI) alkenes: Significant dependence
1057 on the number and nature of double bonds’, *Organic Geochemistry* **42**, pp. 812–822,
1058 doi: <https://doi.org/10.1016/j.orggeochem.2011.04.013>.
- 1059 101. Rontani, J.-F., Belt, S.T., Vaultier, F., Brown, T.A., Massé, G. (2014b),
1060 ‘Autoxidative and Photooxidative Reactivity of Highly Branched Isoprenoid (HBI)
1061 Alkenes’, *Lipids* **49**, pp. 481–494, doi: <https://doi.org/10.1007/s11745-014-3891-x>.
- 1062 102. Rørvik, K.-L., Rasmussen, T.L., Hald, M., Husum, K. (2013), ‘Intermediate water
1063 ventilation in the Nordic seas during MIS 2’, *Geophysical Research Letters* **40**, pp.
1064 1805–1810, doi: <https://doi.org/10.1002/grl.50325>.
- 1065 103. Schmittner, A. (2005), ‘Decline of the marine ecosystem caused by a reduction in
1066 the Atlantic overturning circulation’, *Nature* **434**, pp. 628–633, doi:
1067 <https://doi.org/10.1038/nature03476>.
- 1068 104. Shakun, J.D., Clark, P.U., He, F., Marcott, S.A., Mix, A.C., Liu, Z., Otto-Bliesner,
1069 B., Schmittner, A., Bard, E. (2012), ‘Global warming preceded by increasing carbon
1070 dioxide concentrations during the last deglaciation’, *Nature* **484**, p. 49–54, doi:
1071 <https://doi.org/10.1038/nature10915>.
- 1072 105. Signorini, S.R., McClain, C.R. (2009), ‘Environmental factors controlling the
1073 Barents Sea spring-summer phytoplankton blooms’, *Geophysical Research Letters* **36**,
1074 article L10604, doi: <https://doi.org/10.1029/2009GL037695>.
- 1075 106. Smedsrud, L.H., Esau, I., Ingvaldsen, R.B., Eldevik, T., Haugan, P.M., Li, C., Lien,
1076 V.S., Olsen, A., Omar, A.M., Otterå, O.H., Risebrobakken, B., Sandø, A.B.,

- 1077 Semenov, V.A., Sorokina, S.A. (2013), 'The role of the Barents Sea in the Arctic
1078 climate system', *Reviews of Geophysics* **51**, pp. 415–449, doi:
1079 <https://doi.org/10.1002/rog.20017>.
- 1080 107. Smedsrud, L.H., Halvorsen, M.H., Stroeve, J.C., Zhang, R., Kloster, K. (2017),
1081 'Fram Strait sea ice export variability and September Arctic sea ice extent over the last
1082 80 years', *The Cryosphere* **11**, pp. 65–79, doi: <https://doi.org/10.5194/tc-11-65-2017>.
- 1083 108. Smedsrud, L.H., Ingvaldsen, R.B., Nilsen, J.E.Ø., Skagseth, Ø. (2010), 'Heat in the
1084 Barents Sea: transport, storage, and surface fluxes', *Ocean Science* **6**, pp. 219–234,
1085 doi: <https://doi.org/10.5194/os-6-219-2010>.
- 1086 109. Smik, L., Cabedo-Sanz, P., Belt, S.T. (2016), 'Semi-quantitative estimates of paleo
1087 Arctic sea ice concentration based on source-specific highly branched isoprenoid
1088 alkenes: A further development of the PIP₂₅ index', *Organic Geochemistry* **92**, pp.
1089 63–69, doi: <https://doi.org/10.1016/j.orggeochem.2015.12.007>.
- 1090 110. Søreide, J.E., Carroll, M.L., Hop, H., Ambrose, W.G., Hegseth, E.N., Falk-Petersen,
1091 S. (2013), 'Sympagic-pelagic-benthic coupling in Arctic and Atlantic waters around
1092 Svalbard revealed by stable isotopic and fatty acid tracers', *Marine Biology Research*
1093 **9**, pp. 831–850, doi: <https://doi.org/10.1080/17451000.2013.775457>.
- 1094 111. Stein, R., Fahl, K. (2013), 'Biomarker proxy shows potential for studying the entire
1095 Quaternary Arctic sea ice history', *Organic Geochemistry* **55**, pp. 98–102, doi:
1096 <https://doi.org/10.1016/j.orggeochem.2012.11.005>.
- 1097 112. Stein, R., Fahl, K., Schade, I., Manerung, A., Wassmuth, S., Niessen, F., Nam, S.-I.
1098 (2017), 'Holocene variability in sea ice cover, primary production, and Pacific-Water

- 1099 inflow and climate change in the Chukchi and East Siberian Seas (Arctic Ocean)',
1100 *Journal of Quaternary Science* **32**, pp. 362–379, doi: <https://doi.org/10.1002/jqs.2929>.
- 1101 113. Strass, V.H., Nöthig, E.-M. (1996), 'Seasonal shifts in ice edge phytoplankton
1102 blooms in the Barents Sea related to the water column stability', *Polar Biology* **16**, pp.
1103 409–422, doi: <https://doi.org/10.1007/bf02390423>.
- 1104 114. Stroeve, J.C., Markus, T., Boisvert, L., Miller, J., Barrett, A. (2014), 'Changes in
1105 Arctic melt season and implications for sea ice loss', *Geophysical Research Letters*
1106 **41**, pp. 1216–1225, doi: <https://doi.org/10.1002/2013GL058951>.
- 1107 115. Strong, C., Rigor, I.G. (2013), 'Arctic marginal ice zone trending wider in summer
1108 and narrower in winter', *Geophysical Research Letters* **40**, pp. 4864–4868, doi:
1109 <https://doi.org/10.1002/grl.50928>.
- 1110 116. Syvertsen, E.E. (1991), 'Ice algae in the Barents Sea: types of assemblages, origin,
1111 fate and role in the ice-edge phytoplankton bloom', *Polar Research* **10**, pp. 277–288,
1112 doi: <https://doi.org/10.1111/j.1751-8369.1991.tb00653.x>.
- 1113 117. Tamelander, T., Reigstad, M., Hop, H., Carroll, M.L., Wassmann, P. (2008), 'Pelagic
1114 and sympagic contribution of organic matter to zooplankton and vertical export in the
1115 Barents Sea marginal ice zone', *Deep Sea Research Part II: Topical Studies in*
1116 *Oceanography* **55**, pp. 2330–2339, doi: <https://doi.org/10.1016/j.dsr2.2008.05.019>.
- 1117 118. Thiagarajan, N., Subhas, A.V., Southon, J.R., Eiler, J.M., Adkins, J.F. (2014),
1118 'Abrupt pre-Bølling–Allerød warming and circulation changes in the deep ocean',
1119 *Nature* **511**, p. 75–78, doi: <https://doi.org/10.1038/nature13472>.

- 1120 119. Thornalley, D.J.R., Bauch, H.A., Gebbie, G., Guo, W., Ziegler, M., Bernasconi,
1121 S.M., Barker, S., Skinner, L.C., Yu, J. (2015), 'A warm and poorly ventilated deep
1122 Arctic Mediterranean during the last glacial period', *Science* **349**, pp. 706–710, doi:
1123 <https://doi.org/10.1126/science.aaa9554>.
- 1124 120. Vare, L.L., Massé, G., Belt, S.T. (2010), 'A biomarker-based reconstruction of sea
1125 ice conditions for the Barents Sea in recent centuries', *The Holocene* **20**, pp. 637–643,
1126 doi: <https://doi.org/10.1177/0959683609355179>.
- 1127 121. Vogt, C., Knies, J., Spielhagen, R.F., Stein, R. (2001), 'Detailed mineralogical
1128 evidence for two nearly identical glacial/deglacial cycles and Atlantic water advection
1129 to the Arctic Ocean during the last 90,000 years', *Global and Planetary Change* **31**,
1130 pp. 23–44, doi: [https://doi.org/10.1016/S0921-8181\(01\)00111-4](https://doi.org/10.1016/S0921-8181(01)00111-4).
- 1131 122. Volkman, J. (2003), 'Sterols in microorganisms', *Applied Microbiology and*
1132 *Biotechnology* **60**, pp. 495–506, doi: <https://doi.org/10.1007/s00253-002-1172-8>.
- 1133 123. Volkman, J.K. (1986), 'A review of sterol markers for marine and terrigenous
1134 organic matter', *Organic Geochemistry* **9**, pp. 83–99, doi:
1135 [https://doi.org/10.1016/0146-6380\(86\)90089-6](https://doi.org/10.1016/0146-6380(86)90089-6).
- 1136 124. Volkman, J.K., Barrett, S.M., Blackburn, S.I. (1999), 'Eustigmatophyte microalgae
1137 are potential sources of C₂₉ sterols, C₂₂–C₂₈ *n*-alcohols and C₂₈–C₃₂ *n*-alkyl diols in
1138 freshwater environments', *Organic Geochemistry* **30**, pp. 307–318, doi:
1139 [https://doi.org/10.1016/S0146-6380\(99\)00009-1](https://doi.org/10.1016/S0146-6380(99)00009-1).
- 1140 125. Volkman, J.K., Barrett, S.M., Dunstan, G.A., Jeffrey, S.W. (1993), 'Geochemical
1141 significance of the occurrence of dinosterol and other 4-methyl sterols in a marine

- 1142 diatom’, *Organic Geochemistry* **20**, pp. 7–15, doi: <https://doi.org/10.1016/0146->
1143 [6380\(93\)90076-N](https://doi.org/10.1016/0146-6380(93)90076-N).
- 1144 126. Von Quillfeldt, C.H. (2000), ‘Common Diatom Species in Arctic Spring Blooms:
1145 Their Distribution and Abundance’, *Botanica Marina* **43**, pp. 499–516, doi:
1146 <https://doi.org/10.1515/BOT.2000.050>.
- 1147 127. Walsh, J.E., Fetterer, F., Scott Stewart, J., Chapman, W.L. (2017), 'A database for
1148 depicting Arctic sea ice variations back to 1850', *Geographical Review* **107**, pp. 89–
1149 107, doi: <https://doi.org/10.1111/j.1931-0846.2016.12195.x>.
- 1150 128. Wassmann, P., Ratkova, T., Andreassen, I., Vernet, M., Pedersen, G., Rey, F.
1151 (1999), 'Spring Bloom Development in the Marginal Ice Zone and the Central Barents
1152 Sea', *Marine Ecology* **20**, pp. 321–346, doi: <https://doi.org/10.1046/j.1439->
1153 [0485.1999.2034081.x](https://doi.org/10.1046/j.1439-0485.1999.2034081.x).
- 1154 129. Wassmann, P., Reigstad, M., Haug, T., Rudels, B., Carroll, M.L., Hop, H.,
1155 Gabrielsen, G.W., Falk-Petersen, S., Denisenko, S.G., Arashkevich, E., Slagstad, D.,
1156 Pavlova, O. (2006), 'Food webs and carbon flux in the Barents Sea', *Progress in*
1157 *Oceanography* **71**, pp. 232–287, doi: <https://doi.org/10.1016/j.pocean.2006.10.003>.
- 1158 130. Weinelt, M., Vogelsang, E., Kucera, M., Pflaumann, U., Sarnthein, M., Voelker, A.,
1159 Erlenkeuser, H., Malmgren, B.A. (2003), ‘Variability of North Atlantic heat transfer
1160 during MIS 2’, *Paleoceanography* **18**, article 1071, doi:
1161 <https://doi.org/10.1029/2002PA000772>.

- 1162 131. Willmes, S., Heinemann, G. (2016), 'Sea-Ice Wintertime Lead Frequencies and
1163 Regional Characteristics in the Arctic, 2003–2015', *Remote Sensing* **8**, article 4, doi:
1164 <https://doi.org/10.3390/rs8010004>.
- 1165 132. Winsborrow, M.C.M., Andreassen, K., Corner, G.D., Laberg, J.S. (2010),
1166 'Deglaciation of a marine-based ice sheet: Late Weichselian palaeo-ice dynamics and
1167 retreat in the southern Barents Sea reconstructed from onshore and offshore glacial
1168 geomorphology', *Quaternary Science Reviews* **29**, pp. 424–442, doi:
1169 <https://doi.org/10.1016/j.quascirev.2009.10.001>.
- 1170 133. Wollenburg, J.E., Knies, J., Mackensen, A. (2004), 'High-resolution
1171 paleoproductivity fluctuations during the past 24 kyr as indicated by benthic
1172 foraminifera in the marginal Arctic Ocean', *Palaeogeography, Palaeoclimatology,*
1173 *Palaeoecology* **204**, pp. 209–238, doi: [https://doi.org/10.1016/S0031-0182\(03\)00726-](https://doi.org/10.1016/S0031-0182(03)00726-0)
1174 [0](https://doi.org/10.1016/S0031-0182(03)00726-0).
- 1175 134. Xiao, X., Fahl, K., Müller, J., Stein, R. (2015), 'Sea-ice distribution in the modern
1176 Arctic Ocean: Biomarker records from trans-Arctic Ocean surface sediments',
1177 *Geochimica et Cosmochimica Acta* **155**, pp. 16–29, doi:
1178 <https://doi.org/10.1016/j.gca.2015.01.029>.
- 1179 135. Xiao, X., Fahl, K., Stein, R. (2013), 'Biomarker distributions in surface sediments
1180 from the Kara and Laptev seas (Arctic Ocean): indicators for organic-carbon sources
1181 and sea-ice coverage', *Quaternary Science Reviews* **79**, pp. 40–52, doi:
1182 <https://doi.org/10.1016/j.quascirev.2012.11.028>.
- 1183 136. Yoder, J.A., Ackleson, S.G., Barber, R.T., Flament, P., Balch, W.M. (1994), 'A line
1184 in the sea', *Nature* **371**, pp. 689–692, doi: <https://doi.org/10.1038/371689a0>.

1185 137. Yokoyama, Y., Lambeck, K., De Deckker, P., Johnston, P., Fifield, L.K. (2000),
1186 ‘Timing of the Last Glacial Maximum from observed sea-level minima’, *Nature* **406**,
1187 pp. 713–716, doi: <https://doi.org/10.1038/35021035>.

1188 138. Zamelczyk, K., Rasmussen, T.L., Husum, K., Godtliebsen, F., Hald, M. (2014),
1189 ‘Surface water conditions and calcium carbonate preservation in the Fram Strait
1190 during marine isotope stage 2, 28.8–15.4 kyr’, *Paleoceanography* **29**, pp. 1–12, doi:
1191 <https://doi.org/10.1002/2012PA002448>.

1192

1193

1194

1195

1196

1197

1198

1199

1200

1201

1202

1203

1204

1205 **Figure legends**

1206 Figure 1: Structures of IP₂₅ and HBI II (representing sea ice diatom productivity), as well as
1207 HBIs III and IV (indicative of pelagic diatom productivity). The combined use of HBIs
1208 within proxies for sea ice reconstruction (including P_{III}IP₂₅ and CT models) is illustrated.

1209 Figure 2: Maps of the Barents Sea showing: (a) The main inflow currents carrying AW (via
1210 the NAC, NCaC, and WSC), ArW (PC and ESC), and CW (NCC); (b) Surface and downcore
1211 sample locations. Green and orange circles correspond to surface sediment locations where
1212 HBI with or without additional sterol data were available for comparison with downcore
1213 records, respectively. Both the investigated site and referenced downcore locations are shown
1214 by numbered diamond markers: (1) GS14-190-PC01 (this study and Knies et al., 2018); (2)
1215 JM11-F1-19PC (Hoff et al., 2016); (3) MD95-2010 (Marcott et al., 2011); (4) JM05-85-GC
1216 (Aagaard-Sørensen et al., 2010); (5) JM02-460 GC/PC (Rasmussen et al., 2007); (6)
1217 MSM5/5-712-2 (Müller and Stein, 2014); (7) PS93/006-1 (Kremer et al., 2018a); (8) PS2837-
1218 5 (Wollenburg et al., 2004; Müller et al., 2009); (9) PS92/039-2 (Kremer et al., 2018b); (10)
1219 HH11-09GC (Chauhan et al., 2016); (11) PS2138-1 (e.g. Knies and Stein, 1998; Nørgaard-
1220 Pedersen et al., 2003). Maximum BSIS extent throughout the LGM (at ca. 21 cal kyr BP) is
1221 shown by a filled white area (Hughes et al., 2016). In both maps, dashed and solid black lines
1222 correspond to averaged SpSIC contours (April–June; 1988–2017) of 0% and 15%,
1223 respectively.

1224 Figure 3: HBI concentration profiles for core GS14: (a) IP₂₅ and HBI II, indicative of
1225 sympagic diatom productivity; (b) HBIs III and IV, showing pelagic diatom productivity. A
1226 zoomed-in version of the profile spanning ca. 25–18 cal kyr BP is also shown; (c) P_{III}IP₂₅-
1227 based SpSIC (%) estimates with confidence limits (grey lines) corresponding to the standard
1228 error of calibration (ca. ±11%; Smik et al., 2016), and superimposed categorical CT

1229 predictions of marginal (ca. <10% SpSIC), intermediate (ca. 10–50% SpSIC), and extensive
1230 (>50% SpSIC) sea ice regimes denoted by red diamonds, yellow triangles, and green circles,
1231 respectively. The threshold for summer sea ice occurrence is shown by the horizontal dashed
1232 line. In all plots, coloured background bands constrain the LGM and SEDG (25.8–18.0 cal
1233 kyr BP), HS1 (18.0–16.3 cal kyr BP) and Deglacial (after 16.3 cal kyr BP) intervals – a
1234 rationale for dividing the GS14 record into time slices is provided in the Discussion.
1235 Changepoints significant at a 99.5% confidence level ($p < 0.005$) are shown by vertical red
1236 lines, where upward-pointing dashed arrows apply to the left y-axis only, while a solid line
1237 applies to both the left and right y-axes. Red and blue crosses highlight GS14 and GC08 ^{14}C
1238 AMS dates on the age scale, respectively.

1239 Figure 4: Sterol concentration profiles for core GS14: (a) Brassicasterol and chalinasterol; (b)
1240 Campesterol and β -sitosterol; (c) Dinosterol; (d) Cholesterol. In all plots, coloured
1241 background bands constrain the LGM and SEDG (25.8–18.0 cal kyr BP), HS1 (18.0–16.3 cal
1242 kyr BP) and Deglacial (after 16.3 cal kyr BP) time slices. Changepoints significant at a 99.5%
1243 confidence level ($p < 0.005$) are shown by vertical red lines, where upward or downward
1244 pointing dashed arrows apply to the left and right y-axis, respectively, while a solid line
1245 applies to both left and right y-axes. Red and blue crosses highlight GS14 and GC08 ^{14}C
1246 AMS dates on the age scale, respectively.

1247 Figure 5: Planktic $\delta^{18}\text{O}$ of *N. pachyderma* sin. (black line with circle markers) and IRD data
1248 (green line) for core GS14, obtained from Knies et al. (2018). Red and blue crosses highlight
1249 GS14 and GC08 ^{14}C AMS dates on the age scale, respectively.

1250 Figure 6: Concentration distributions during the LGM (with SEDG), HS1, and Deglacial for:
1251 (a) HBIs; (b) Sterols. Error bars denote ± 1 sample SD in each case. Blue and red boxes with
1252 outgoing arrows show plot areas zoomed in for clarity for HBIs and sterols, respectively.

1253 Figure 7: Relative abundance distributions during the LGM (with SEDG), HS1, and
1254 Deglacial for: (a) HBIs, with comparisons to modern distributions reported in Barents and
1255 Norwegian Sea surface sediments characterised by contrasting sea ice regimes (**Fig. 1b**); (b)
1256 Sterols, with comparisons to surface sedimentary distributions analogous to those in (a). Error
1257 bars denote ± 1 sample SD for each biomarker, while the sample size n is shown in red above
1258 each distribution.

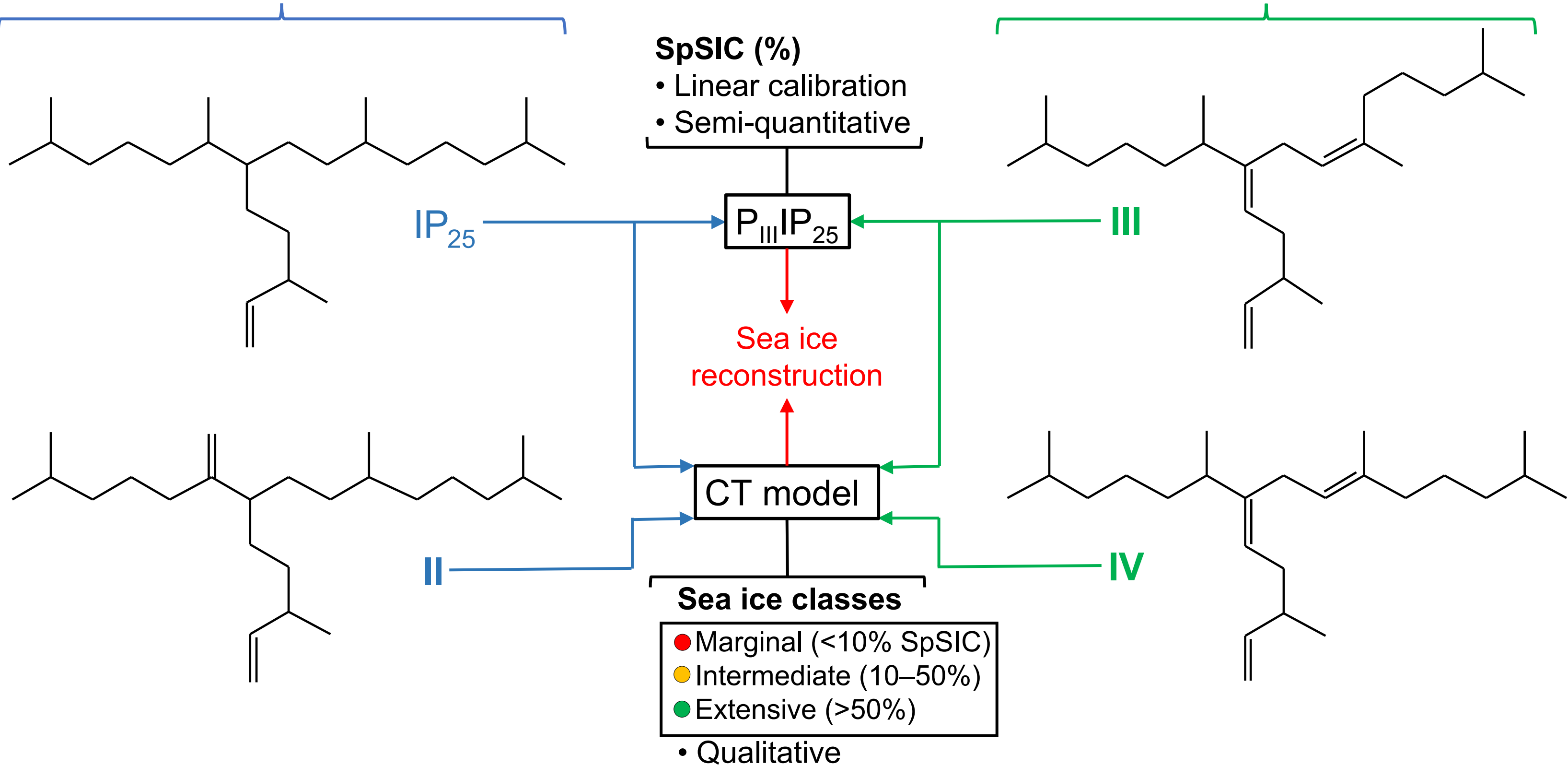
1259 Figure 8: Conceptual representation of sea ice and productivity conditions at the southwestern
1260 Barents Sea continental slope throughout: (A) The LGM and SEDG (25.8–18.0 cal kyr BP);
1261 (B) The HS1 (18.0–16.3 cal kyr BP); (C) The Deglacial (16.3 cal kyr BP onwards). Seasonal
1262 sea ice conditions inferred from SpSIC (%) and the CT model are illustrated during winter
1263 (October–March), spring (April–June) and summer (July–September). Red and blue arrows
1264 correspond to AW and meltwater fluxes, respectively, where line width increases with flow
1265 strength. Orange arrows represent solar insolation.

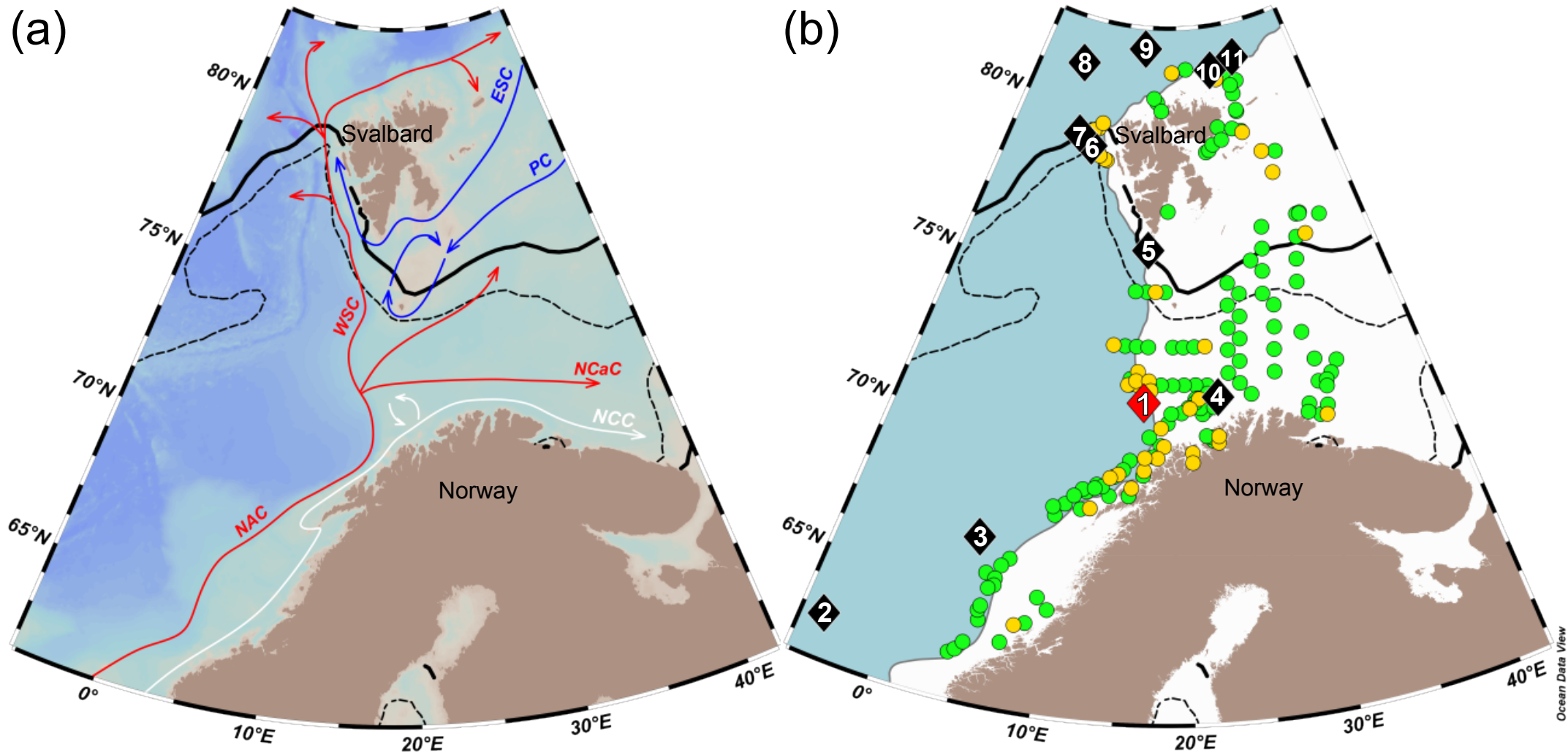
1266 **Tables**

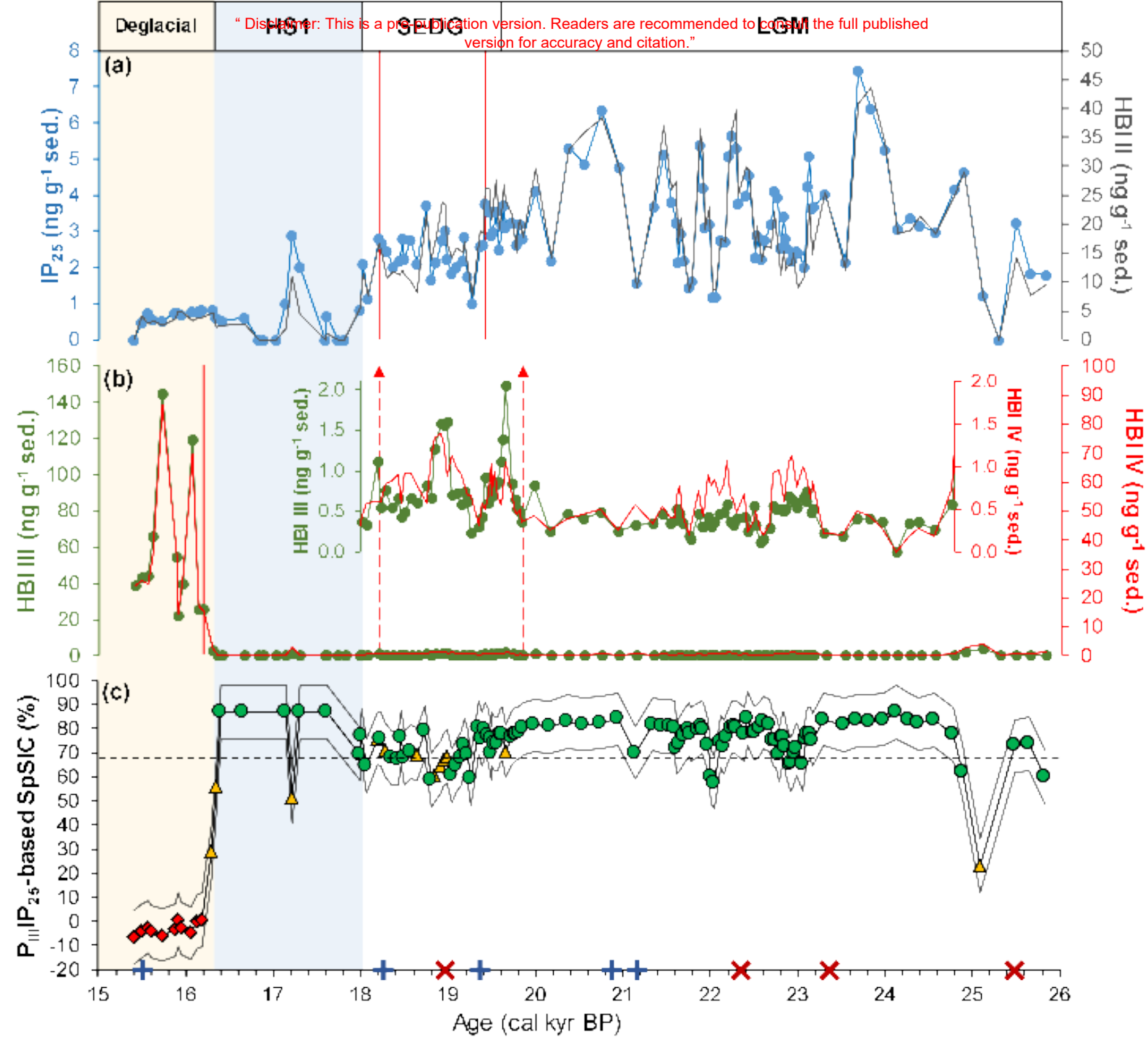
1267 Table 1: Uses and potential limitations of HBI and sterol lipids utilized as biomarkers of sea
1268 ice and primary productivity regimes in the current study.

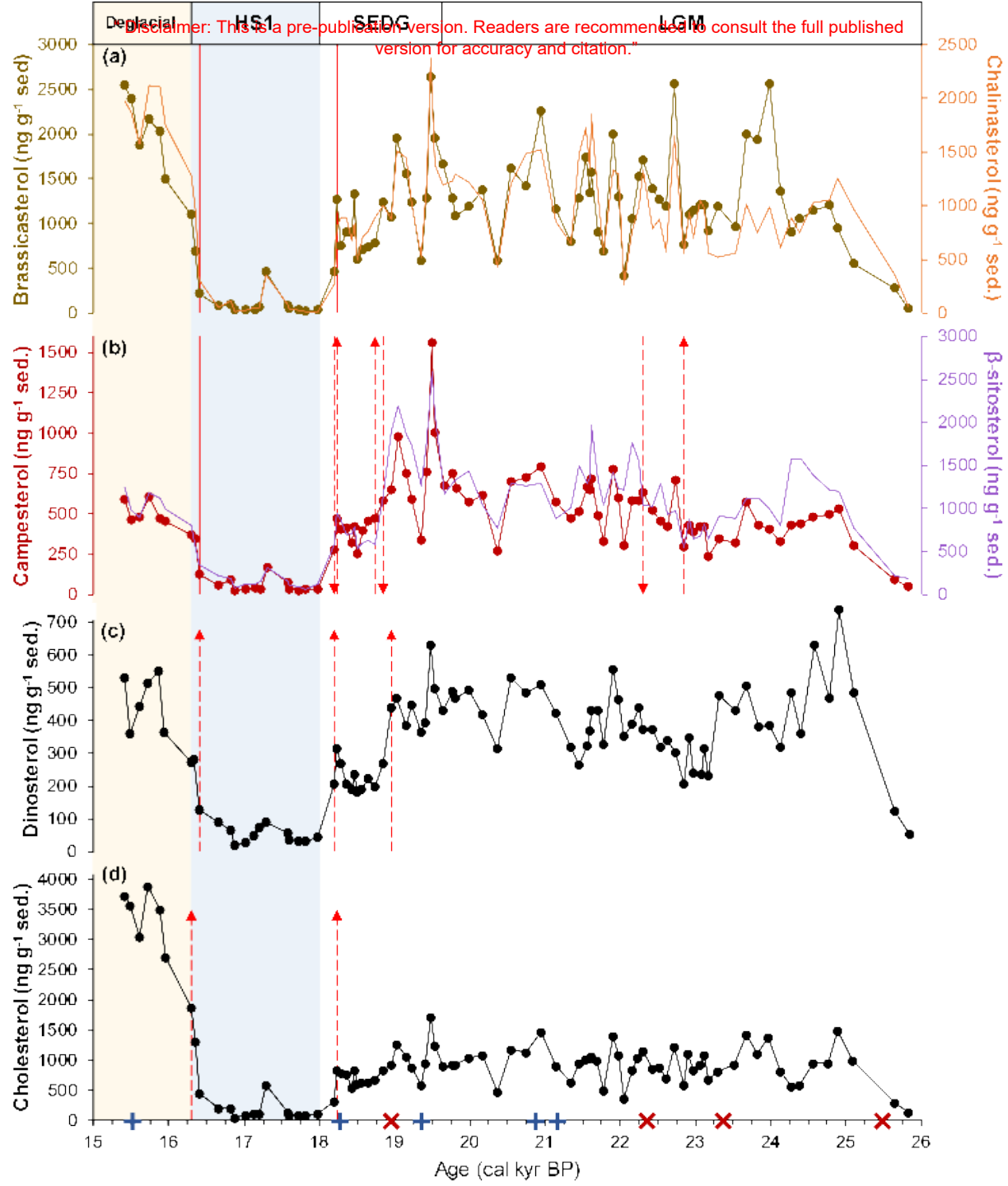
Sympagic biomarkers (sea ice algal productivity)

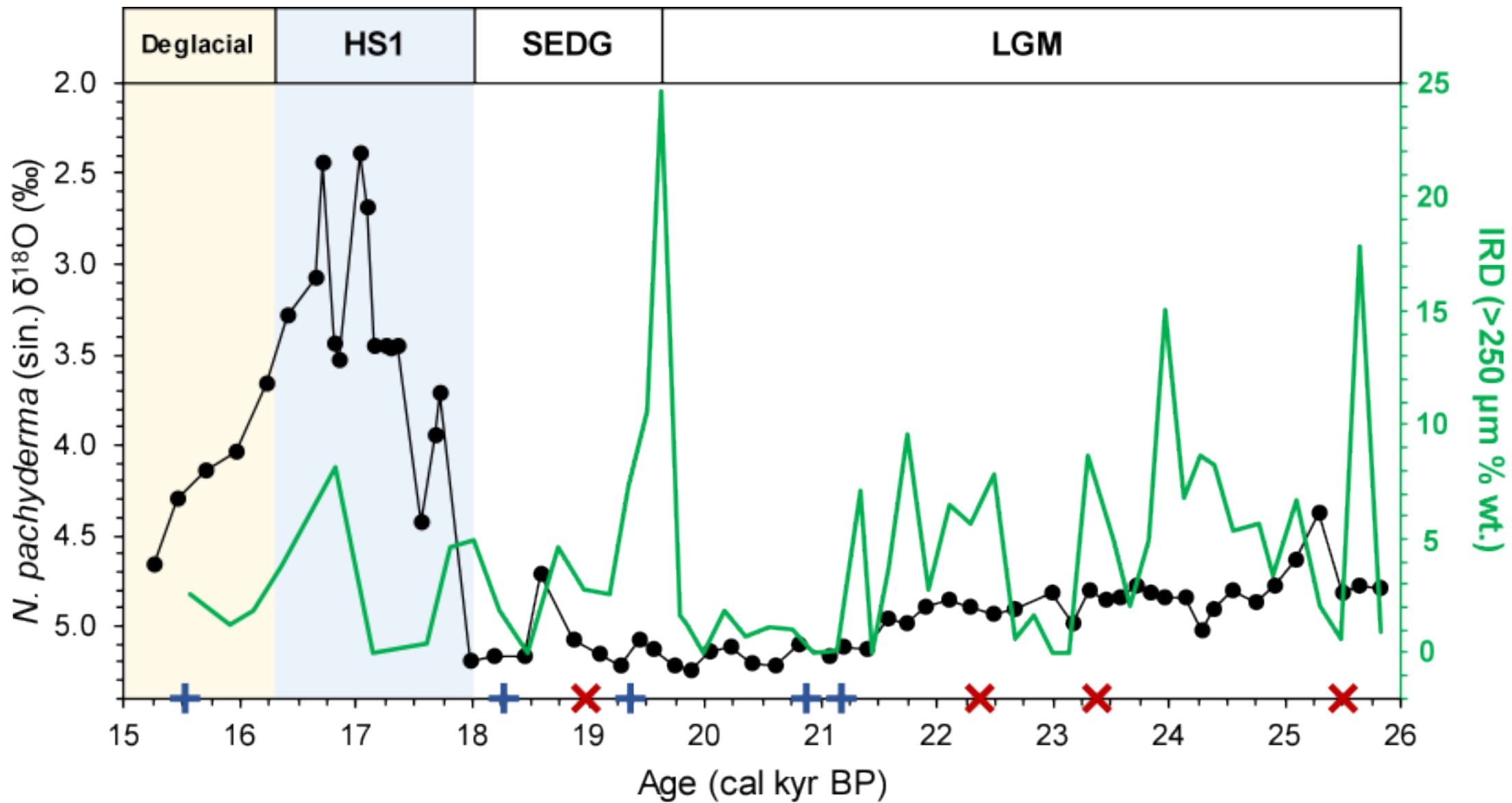
Pelagic biomarkers (open water productivity)



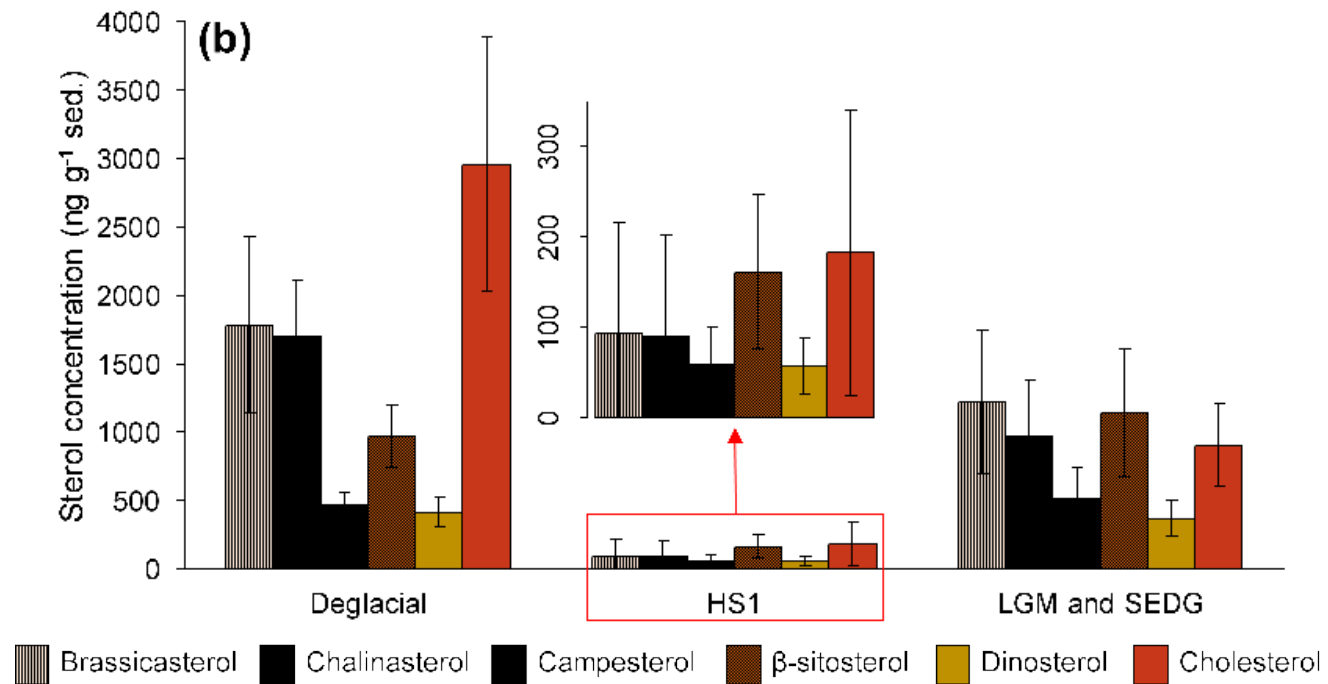
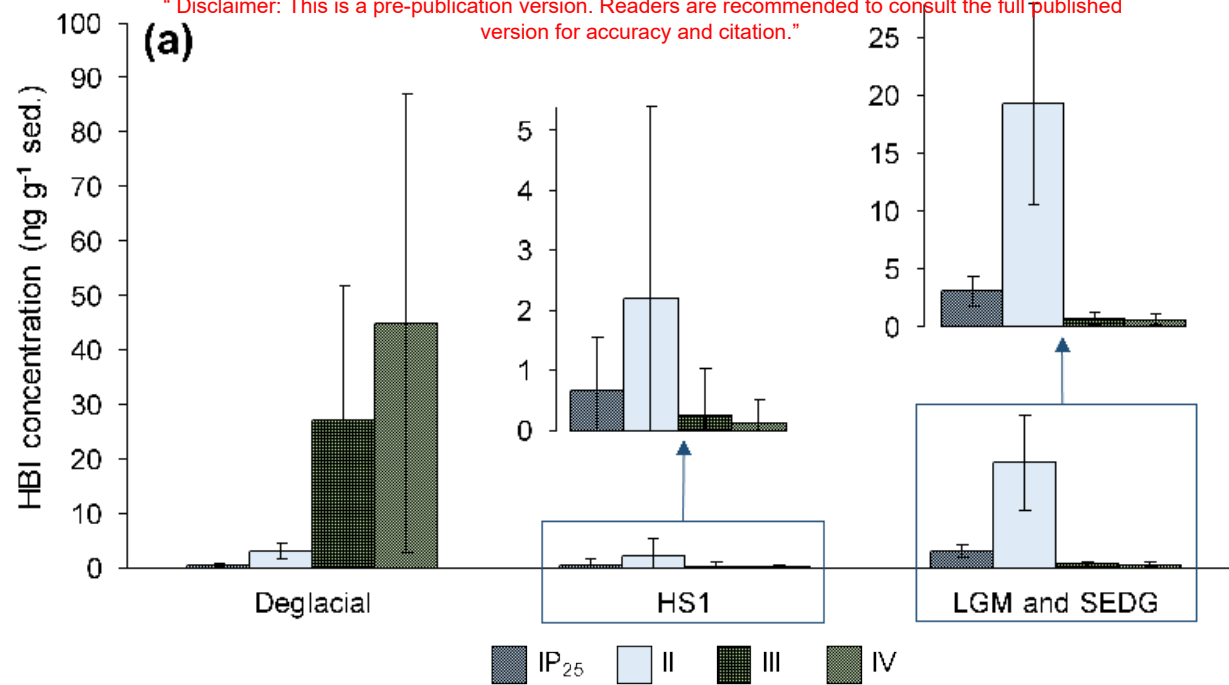


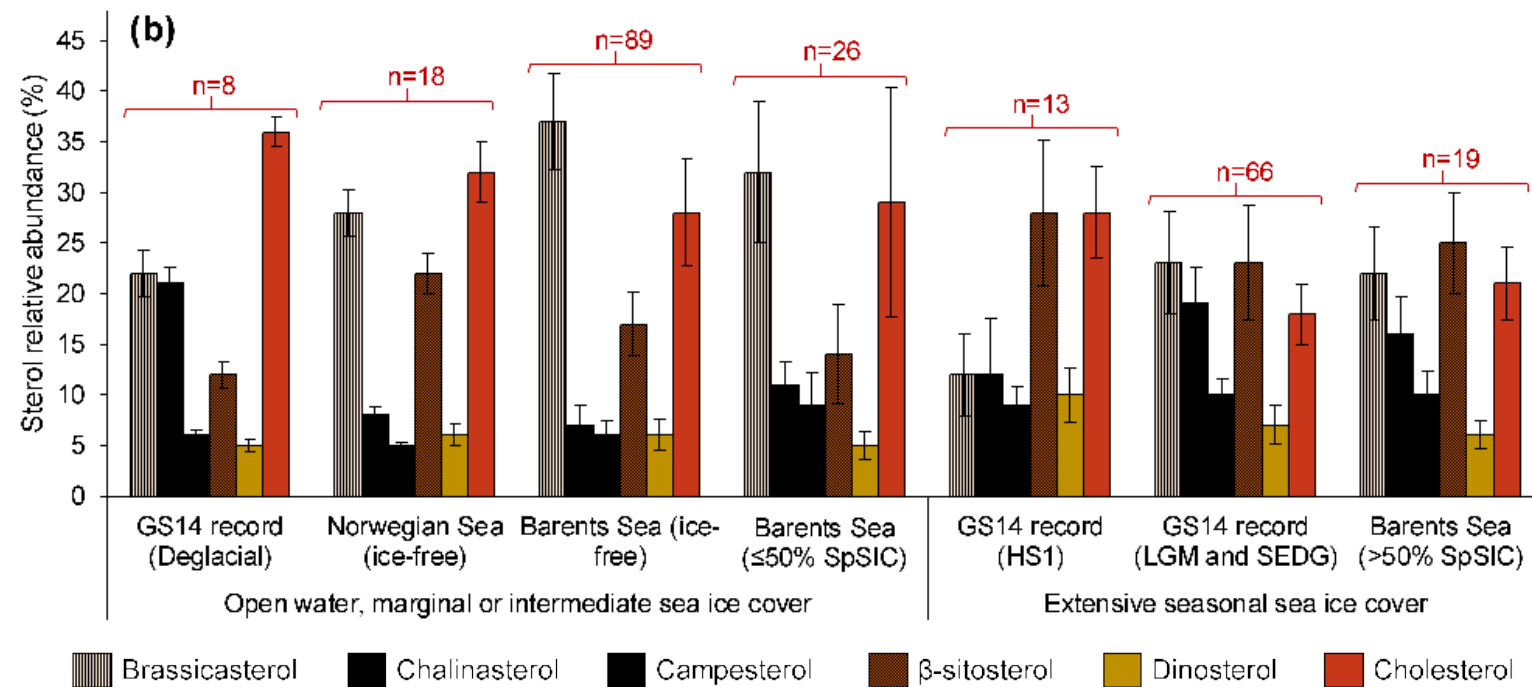
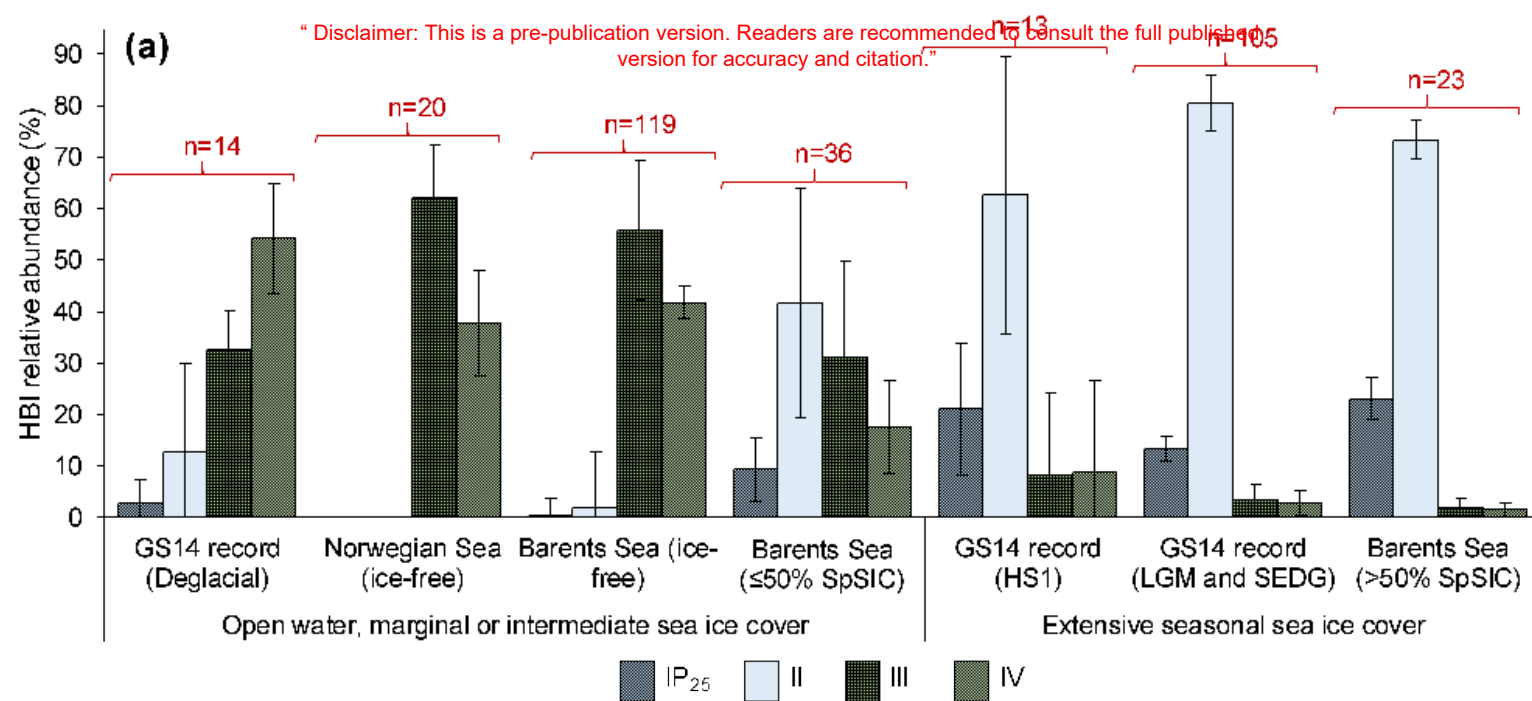






“Disclaimer: This is a pre-publication version. Readers are recommended to consult the full published version for accuracy and citation.”





HBIs	Common use(s)	Potential limitation(s)	Present interpretation	References
IP ₂₅ and II	Source-specific, co-produced diatom proxies of seasonal Arctic sea ice ^{1, 2} . Stable within sedimentary record and resistant to photodegradation and autoxidation ³ .	Require concurrent analysis of an open-water biomarker(s) to distinguish perennial ice and open water settings ^{4, 5, 6, 7} . Only represent productivity of minor sympagic diatoms ^{1, 2} .	Used as indicators of sympagic diatom productivity within sea ice, where absolute concentrations and relative abundances increase with longer seasonal sea ice duration.	Belt et al. (2015 ⁵ , 2016 ² , 2017 ⁹) Brown et al. (2014b) ¹ Köseoğlu et al. (2018a,b) ⁷ Müller et al. (2011) ⁴ Ringrose (2012) ⁸ Rontani et al. (2011, 2014b) ³ Smik et al. (2016) ⁶
III and IV	Ubiquitous pelagic diatom proxies vastly enhanced during the spring MIZ phytoplankton bloom, and limited under extensive ice conditions ^{5, 6, 7} . III used to derive P _{III} IP ₂₅ -based SpSIC estimates ^{5, 6} , and IV used for CT predictions of sea ice cover ⁷ .	Increased degradation rates relative to IP ₂₅ and II, at least under laboratory conditions ³ . IV (<10%) detected in sea ice, while all but one <i>in-situ</i> sources in the Arctic (<i>Rhizosolenia setigera</i>) are still unknown ⁹ .	Used as indicators of pelagic diatom productivity in the photic zone of the water column. Absolute concentrations and relative abundances increase under highly-productive conditions.	Reviews: Belt and Müller (2013) Belt (2018)
Sterols				
Brassicasterol	A major constituent of marine algae and indicative of general productivity ¹⁰ .	Present in sea ice ¹¹ .	Due to their reduced source-specificity, variability of all absolute sterol concentrations was interpreted as a general indicator of changes in marine productivity.	Belt et al. (2013, 2018) ¹¹ Boon et al. (1979) ¹⁵ Hassett and Crockett (2009) ¹⁹ Huang and Meinschein (1976) ¹⁴ Mühlebach et al. (1999) ¹⁸ Nichols et al. (1990) ¹⁶ Rampen et al. (2010) ¹⁰ Rontani et al. (2014a, 2016) ¹² Volkman et al. (1993) ¹⁷
Chalinasterol	An indicator of marine diatom productivity as the dominant sterol in many centric and pennate diatoms ¹⁰ .	Susceptible to photodegradation and autoxidation ¹² ; Found in other algae (e.g. cryptomonads), and in sea ice ^{11, 13} .	Comparison of sterol relative abundance distributions downcore to those of surface sediments was used to identify similarities and differences between paleo and more recent/contemporary settings characterised by contrasting sea ice and/or productivity conditions.	Review: Volkman (1986) ¹³
Campesterol and β -sitosterol	Commonly associated with terrigenous input from vascular plants ¹⁴ .	Found in many diatoms, where β -sitosterol often dominates the sterol assemblage ¹⁰ .		
Dinosterol	A common biomarker of dinoflagellate productivity ¹⁵ .	Detected as a minor constituent of diatoms (including sympagic) in polar settings ¹⁶ and cultures ¹⁷ .		
Cholesterol	High proportional abundance can indicate increased marine faunal productivity ¹³ .	Ubiquitous amongst vertebrates ^{18, 19} and diatoms ¹⁰ .		